THE UNIVERSITY OF MANITOBA

A NUMERICAL ANALYSIS ON CREEP CRACK PROPAGATION

by

Zhen-Hua Zhai

A thesis
presented to the University of Manitoba
in partial fulfillment of the
requirements for the degree of
Master of Science
in
Department of Mechanical Engineering

Winnipeg, Manitoba, 1983

A NUMERICAL ANALYSIS ON CREEP CRACK PROPAGATION

BY

ZHEN-HUA ZHAI

A thesis submitted to the Faculty of Graduate Studies of
the University of Manitoba in partial fulfillment of the requirements
of the degree of

MASTER OF SCIENCE

I hereby declare that I am the sole author of this thesis.

I authorize the University of Manitoba to lend this thesis to other institutions or individuals for the purpose of scholarly research.

Zhen-Hua Zhai

I further authorize the University of Manitoba to reproduce this thesis by photocopying or by other means, in total or in part, at the request of other institutions or individuals for the purpose of scholarly research.

Zhen-Hua Zhai

The University of Manitoba requires the signatures of all persons using or photocopying this thesis. Please sign below, and give address and date.

ACKNOWLEDGEMENT

The author extends her most sincere thanks to Dr. T.R. Hsu of the Department of Mechanical Engineering in the University of Manitoba for his valuable assisstance, advice and guidance in supervising this thesis. Thanks are also extended to Dr. J. Shewchuk, Dr. M.N. Bassim and Prof. R. Schilling of the same department and Dr. L. Simpson of Atomic Energy Canada Ltd. for their valuable suggestions and advice.

Assistance from some of the auther's colleagues, Mr. Y.J. Liu, Dr. Y.J. Kim is also appreciated.

The financial support by the Natural Science and Engineering Research Council of Canada and the computing facilities provided by the University of Manitoba Computer Center are acknowledged as well.

The auther is indebted to the goverment of the People's Republic of China for its partial support on this study program at its initial stage.

ABSTRACT

The subject of creep fracture is rather empirical at the present stage. The present study attempts to apply the finite element method to simulate the crack propagation process under high temperature where creep becomes very significant. A plate in plane stress state with a line crack was used for the case studies. Besides visco-elastic creep, plasticity was also considered, which was absent in many previous numerical analyses in this field. In the finite element modelling of the creep crack growth, the "breakable element" concept and the corresponding stress relaxation of the broken elements were introduced. The correlation between the crack growth rate $\dot{a}$ and the parameter C* was also included. The results are compared with both numerical and experimental works by other researchers. It is found that the results from this study are closer to the experimental results than those by other numerical studies.

CONTENTS

LIST OF FIGURES

LIST OF TABLES

NOMENCLATURE

a, a_o	Crack length and initial crack length respectively
Δa	Increment of crack length
$[B]$	Stress-displacement transformation matrix
$[C]$	Stress-strain constitutive matrix
$[C_e]$	Elastic matrix
$[C_{ep}]$	Plastic matrix
E	Elastic modulus
E'	Plastic modulus
F	Von Mises plastic potential function
$\{F\}$	Force vector
H'	Equivalent plastic modulus
J	Path-independent contour integral
J_2	Second deviatoric stress invariant
K	Work hardening parameter or stress intensity factor
K_c,K_{IC}	Plane stress and plane strain fracture toughnesses
$[K_e]$	Element stiffness matrix
$[K]$	Global stiffness matrix
n	Power hardening coefficient in the stress-strain law or exponent in Norton's creep law
$[N]$	Displacement transformation matrix
$\{dp\}$	Increment of mechanical load vector

$\{dp_c\}$	Increment of pseudo creep load vector
Q	Activation energy
R	Crack growth resistance or universal gas constant
ds	Differential element of an arc length along the contour path
t	Time
T	Surface traction vector for J-integral evalution or absolute temperature
$\{u\}$	Displacement vector
$\{u_o\}$	Nodal displacement vector
U	Potential energy
v	Volume of the element
W	Strain energy density function
x,y,z	Coordinate system
r, θ	
β	Constant
$\mathring{\beta}$	Positive parameter depending on the loading history
Γ	Contour path in J-integral and C* parameter evaluation
δ	Additional crack length
ε	Strain
ε_{ext}	Extrapolated strain at the crack tip
$\bar{\varepsilon}, \bar{\varepsilon}_p$	Effective strain and effective plastic strain
ε_{rup} or ε_f	Rupture strain
$\{\varepsilon\}, \{\Delta\varepsilon\}$	Strain and incremental strain vectors respectively
$\dot{\bar{\varepsilon}}^c$	Effective creep strain rate

$\{\dot{\varepsilon}\}$	Strain rate vector
$\{\dot{\varepsilon}^c\}$	Creep strain rate vector
$\{\dot{\varepsilon}_{ep}\}$	Elastic-plastic strain rate
θ	Angle between the crack line and crack initiation direction
$d\lambda$	Proportionality factor
ν	Poisson's ratio
ψ	Creep potential function
σ_{xx}, σ_{yy} σ_{xy}, etc	Stress components
σ_g	Gross section stress
$\bar{\sigma}$	Effective stress
σ_{ys} or σ_y	Yield strength of the material
σ'	Deviatoric stress components
$\{\sigma\}$	Stress vector
τ_y	Yield strength in pure shear
COA	Crack Opening Angle
CTOA	Crack Tip Opening Angle

Chapter I

INTRODUCTION

1.1 INTRODUCTION

Through a series of accidents and casualties, it was gradually discovered that pre-existing flaws in materials could initiate cracks and fractures. This discovery led to the development of fracture mechanics.

Fracture mechanics approach provides a technique where material behavior is analyzed with the assumption of pre-existing crack-like defects. Analysis of material fracture frequently consists of three individual steps: the initiation, propagation of cracks and the final failure. Engineering fracture mechanics can usually deliver the methodology to compensate the inadequancies of conventional design concepts.

On the other hand, the importance of allowing for creep in the design of certain components operating under sustained loading at elevated temperatures has long been recognised. It was found that failure occurs by the initiation and propagation of a single macroscopic flaw at high temperature more easily than at room temperature. This problem is especially important for those structural components involved in modern power plants and nuclear reactors operating

at elevated temperature. Many of these components are of such large sizes that current technology in the inspection and repairment preclude the assumption of a defect free structure. In these cases, the material behavior might better be chacterized by an analysis which accounts for these defects. The very early report was given by Kaufman and Holt [1]. They reported on their findings of time dependent crack growth in 2219-T851 plate at elevated temperatures. As a result of those findings, a program was initiated to investigate the significance of this phenomenon on the service ability of materials utilizing fracture mechanics.

1.2 LITERATURE SURVEY

There are quite a few publications on creep fracture mechanics, a comprehensive review in this area was given in 1980 by Fu [2].

One of the main objectives of the study of creep fracture mechanics is to establish a mathematical relationship between the creep crack growth rate $\dot{a}$ and some suitable parameter. In some early works, based on the application of linear elastic fracture mechanics techniques to brittle fracture, Neat and Sivens, Floreen and James et al [3-5] showed that creep crack growth rate could be expressed as a power function of elastic stress intensity factor K. This was supported by Kenyon and Yokobori [6,7]. Later, people started to search in the non-linear fracture mechanics area.

Net section stresses σ_{net} had been proposed by Harrison and Sandor, Nicho and Formby [8,9] and several other researchers [10,13] as another parameter which can be used to describe creep crack growth. Freeman [14] found the reference stress to be a better parameter for some materials and Haigh, Vitek and Pilkington [15-17] used the crack opening displacement rate to describe the crack growth behavior. A number of authors [18-21] attemped to extend the J-integral concept to the creep condition. They defined a parameter C* to deal specially with the visco-elastic creep fracture problems. C* is a power or energy rate line integral under small scale yielding, it is interpreted as the energy rate difference between crack lengths a and a_1.

The C* method holds great promise for design calculations and is widely studied. Though it was proposed under the elastic or very limited elastic-plastic conditions, it has been modified in various ways to suit large plasticity cases. It can be calculated using finite element methods or by some empirical formulae as well as measured empirically in constant displacement rate tests.

Many researchers have tried to summarize and explain the applicability and limitation of all these parameters. The general conclusion is that creep crack growth rates correlate well with K only for brittle materials and correlate better with σ_{net} for ductile materials. For the in between cases, C* or modified C* is a better parameter to correlate the creep crack growth rates [22-25].

Recently, a few new parameters were proposed. In 1981, a parameter $(\Delta T)_c$ was developed by Atluri [26] which is a path independent vector integral and subsequently had been examined in greater detail by Stonesifer and Atluri [27,28]. Through their analytical work, they concluded that $(\Delta T)_c$ is a parameter which bridges the gap between K controlled growth and C* controlled growth and it can be applied to problems of non-steady creep as well as steady-state creep and so it has some advantages over the more commonly used C* parameter which can only be applied to steady-state creep.

Liu and Hsu [29] studied another parameter C_g^* which modified the C* parameter by adding a plastic energy rate integral term to the C* formulation and claimed that this parameter can uniquely characterize creep crack growth behavior from the small scale plasticity to extensive scale plasticity. They concluded that this C_g^* overcomes the inconsistency and the often-confused uses of parameters K, C* and σ_{net} in characterizing the crack behavior for different creep stages.

On the theoretical and analytical side, Goldman and Hutchinson [30] proved that under steady state creep conditions, there exists a strain rate singularity at the crack tip which can be characterized by the C* parameter. Riedel [31] discussed the creep behavior near the crack tip at different stages of creep deformation. Hui. and Riedel [32] derived the asymptotic stress and strain fields near the

crack tip of a slowly growing crack and discussed the stress and strain singularity of this field. McCartney [33] applied a continuum energy balance approach to the creep fracture of both linear and non-linear materials. With a generalized creep damage hypothesis, Kubo et al [34] proposed an analytical method based on singular stress strain field near the crack tip. McCartney [35] proposed a crack growth law for linear visco-elastic solids by using the Dugdale model of small yielding. Other models have also been proposed, such as critical strain model by Barnby [36], plastic zone size modal by To [37], continuous rupture model by Purushothaman and Tien [38] and critical COD model by Vitek [39] etc.

Taira and Ohtani [12,40] applied the finite element method to simulate the process of creep crack growth under a critical strain criterion and compared it with their experimental work. This will be discussed in detail in Chapter 7. Stonesifer and Atluri [27,28] also performed finite element analysis under the uniformly applied displacement rates at the top and bottom edges of a compact tensile specimen. In their analysis both C* and crack propagation rate $\dot{a}$ were assumed to be constant.

As for the mechanism of creep crack growth from a standpoint of microstructure, a review on analytical treatments of creep crack growth due to vacancy diffusion and condensation was given by Leeuwen [41]. It is agreed that under creep conditions the diffusion of vacancies towards a crack

or a void and their condensation there would contribute to the crack growth. Based on the crack tip stress field in a creeping body and on models for microvoid growth, Riedel [42] showed that at low level of C*, the voids growth mechanism prevails by diffusion whereas at high C*-values the voids grow mainly due to creep.

1.3 OBJECTIVE OF THIS THESIS

A review of the literature of creep fracture shows that experimental studies were dominant during the past years. Though there were some theoratical analysis, most of them were limited to the stress strain analysis around a crack. The analytical analysis of creep crack growth is complicated not only by the non-linear creep deformation of the whole structure but also by the plastic region developed at the crack tip. To the author's knowledge, in the very few finite element analyses of the creep crack propagation problem, elastic-plastic analysis was not considered. It would be interesting to see how this simplification would affect the results. The objective of this thesis is to approach the creep crack growth by another way in which an elastic-plastic analysis is included.

In this thesis, the creep deformation will be converted to a corresponding "pseudo-creep load" and added to an elastic-plastic analysis by the finite element method. When the strain at the crack tip reaches the value ε_f which is

called a rupture strain, the crack starts to grow. To simulate the real process of the crack growth, the "breakable elements" [69,70] will be used which does not break at once but gradually. After the element is broken the reaction force at the former crack tip will be given back to the structure also gradually in a form of relaxation.

The results will consist of the stress and strain fields in the vicinity of the crack tip, the profile of the crack, the mathematical relationship between the crack growth rate $\dot{a}$ and the C* parameter and the size and shape of the plastic zone. The results will show that the method used in this thesis is acceptable and the program works well. Through this investigation, one may find that it is quite possible to use a numerical method to establish the relationship between the creep crack growth rate $\dot{a}$ and the C* parameter.

Chapter II

ELASTIC-PLASTIC STRESS STRAIN ANALYSIS BY FINITE ELEMENT ANALYSIS

2.1 REVIEW OF THE BASIC EQUATIONS IN FINITE ELEMENT METHOD

When a solid is loaded at a stress level beyond its elastic limit, the relationship between the stress and strain is not linear any more. Various elastic-plastic analysis methods have been proposed and most of them are expressed in differential forms. Thus it is impossible to avoid a step by step solution.

The finite element method was developed to meet the demand for the numerical solutions of this types of engineering analyses problems and hence this method was also used in this analysis.

The basic idea in finite element is to discretize a body or a structure of complex geometry into an equivalent system of smaller bodies, or units. Instead of solving the problem for the entire body in one operation, the solutions are formulated for each constituent unit and then combined to obtain the solution for the original body or structure.

In this analysis, the finite element displacement method is used and hence is presented in this section.

For each unit or element, the displacement $\{ u \}$ at any point in the element can usually be related to the nodal displacement $\{ u_0 \}$ by

$$\{ u \} = [N] \{ u_o \} , \qquad (2.1.1)$$

where [N] is called a displacement transformation matrix or a shape function.

If { ε } is the vector of the relevant strain components at an arbitrary point within the finite element, we use the strain displacement equations and the displacement model to give:

$$\{ \varepsilon \} = [B] \{ u_o \} , \qquad (2.1.2)$$

where [B] is a matrix involving the derivatives of the shape function [N] with respect to the nodal coordinates.

If { σ } is the vector of stress corresponding to the strain { ε }, we may get a stress-strain relation following the generalized Hooke's law:

$$\{ \sigma \} = [C] \{ \varepsilon \} = [C] [B] \{ u_o \} \qquad (2.1.3)$$

where [C] is a matrix of material property constants and is usually called elasticity matrix.

Suppose one element is loaded by some external forces { F }, the work done by the nodal forces { F } is equal to the sum of the products of the forces and the displacements in the forces direction:

$$W_e = \{ u_o \}^T \{ F \} \ , \qquad (2.1.4)$$

where $\{ u_o \}$ is the nodal displacement vector.

The strain energy due to internal work done by the associated stress and strain fields is:

$$\begin{aligned} W_i &= \int_v \{ \varepsilon \}^T \{ \sigma \} \, dv \\ &= \int_v \{ \varepsilon \}^T [C] \{ \varepsilon \} \, dv \\ &= \int_v ([B] \{ u_o \})^T [C] [B] \{ u_o \} \, dv \\ &= \int_v \{ u_o \}^T [B]^T [C] [B] \{ u_o \} \, dv \end{aligned} \qquad (2.1.5)$$

where v represents the volume of the element.

According to the variational principle, the functional

$$\Pi = W_i - W_e$$

will be stationary when

$$\frac{\partial \Pi}{\partial \{u\}} = 0 \ ,$$

or in this case

$$\frac{\partial \Pi}{\partial \{u_0\}^T} = \frac{\partial W_i}{\partial \{u_0\}^T} - \frac{\partial W_e}{\partial \{u_0\}^T} = 0 \ .$$

By substituting the expresions for W_i and W_e in Eqs.(1.1.4) and (1.1.5) into the above relation, we may obtain

$$\frac{\partial}{\partial \{u_0\}^T} \left(\{u_0\}^T \{F\} \right) - \frac{\partial}{\partial \{u_0\}^T} \left(\int_V \{u_0\}^T [B]^T [C] [B] \{u_0\} \, dv \right) = 0 \quad .$$

Since $\{ u_o \}$ are the nodal displacements which are independent of coordinates, they may be moved out from the integral. The following equation can thus be derived:

$$\{ F \} = \int_V [B]^T [C] [B] \, dv \, \{ u_o \} \qquad (2.1.6)$$

Let

$$[K_e] = \int_V [B]^T [C] [B] \, dv \ , \qquad (2.1.7)$$

$[K_e]$ is called stiffness matrix.

Every element has its own stiffness matrix. After all the stiffness matrices are evaluated, the stiffness for the assemblage can be formed by summing up all the element matrices to give:

$$[K] = \sum_{e=1}^{E} [K_e] \quad , \qquad (2.1.8)$$

The equilibrium equations for the assemblage are now obtained as

$$[K] \{ u_o \} = \{ F \} \quad . \qquad (2.1.9)$$

By solving these equations, the displacements at each nodal point can be obtained, then from (1.1.2) and (1.1.3) the strain and stress in each element can be determined.

2.2 YIELD CONDITION

The Von Mises yield condition has been accepted as the most practical and reliable yield criteria. For most engineering materials, when the Von Mises plastic potential at one point of a material becomes equal or greater than zero, plastic deformation occurs.

The general form of the Von Mises plastic potential is :

$$F = F (\{ \sigma \} , K , T , \{ \dot{\varepsilon} \}) \quad . \qquad (2.2.1)$$

where K = the usual hardening parameter,

$\{ \sigma \}$ = stress vector,

T = temperature and

$\{ \dot{\varepsilon} \}$ = strain rate.

For an isotropic material, F is defined by

$$F = J_2 - \tau_y^2 = J_2 - \frac{1}{3} \sigma_y^2 \quad , \qquad (2.2.2)$$

where τ_y and σ_y are the yield stress in pure shear and in uniaxial tension respectively, J_2 is the second stress invariant

$$J_2 = \frac{1}{2} \sigma'_{ij} \sigma'_{ij} \qquad (2.2.3)$$

and σ'_{ij} is the deviatoric stress components defined as:

$$\sigma'_{ij} = \sigma_{ij} - \sigma_m$$

$$= \sigma_{ij} - \frac{1}{3} \sigma_{ii} \quad .$$

According to Von Mises criterion, plastic yielding takes place when:

$$F = 0 \quad ,$$

i.e.

$$J_2 - \frac{1}{3}\sigma_y^2 = 0 \qquad (2.2.4)$$

or

$$J_2 = \frac{1}{3}\sigma_y^2 \quad .$$

From (2.2.3) we obtain

$$\frac{3}{2}\sigma'_{ij}\,\sigma'_{ij} = \sigma_y^2 \quad . \qquad (2.2.5)$$

Since the effective stress is defined as

$$\bar{\sigma} = \{ \frac{1}{2} [(\sigma_{11} - \sigma_{22})^2 + (\sigma_{22} - \sigma_{33})^2 + (\sigma_{11} - \sigma_{33})^2] + 3 (\sigma_{12}^2 + \sigma_{23}^2 + \sigma_{13}^2) \}^{\frac{1}{2}}$$

$$= (\frac{3}{2}\sigma'_{ij}\,\sigma'_{ij})^{\frac{1}{2}} \quad . \qquad (2.2.6)$$

for a multi-axially loaded solid, it is easily observed from (2.2.5) and (2.2.6) that

$$\bar{\sigma} = \sigma_y \quad . \qquad (2.2.7)$$

which is the yield criterion used in this analysis.

2.3 MATERIAL CONTITUTIVE RELATION

The relationship between the effective stress and the effective plastic strain for a material subjected to plastic deformation is usually determined from experiments. Functions which can describe experimentally established continuous stress vs. strain curves are necessary for the analysis. Hsu et al [43] have proposed such a function which can cover the entire stress vs. strain regime. This function describe a sharp turn at the conjunction of the elastic and plastic parts of the stress-strain curve which is closer to the true stress-strain curve.

$$\bar{\sigma} = \frac{\bar{E}\,\bar{\varepsilon}}{\left\{ 1 + \left[\frac{\bar{E}\,\bar{\varepsilon}}{\left(1 - \frac{\bar{E}'}{\bar{E}} \right) \bar{\sigma}_{kink} + \bar{E}'\,\bar{\varepsilon}} \right]^{n} \right\}^{1/n}} \qquad (2.3.1)$$

where

$$\bar{E} = \frac{3E}{2(1+\nu)} \quad ,$$

$$\bar{E}' = \frac{3E'}{3 - \frac{(1-2\nu)E'}{E}}$$

with E and E' to be the respective moduli of elasticity and plasticity from a uni-axial stress vs. strain curve and

$\bar{\sigma}_{kink}$ = the stress at which the elastic line intersects with the tangent of the plastic curve as shown in Fig.1.

By differentiating (2.3.1), one may obtain a tangent modulus E_t:

$$E_t = \frac{d\bar{\sigma}}{d\bar{\varepsilon}} = \frac{\bar{E}\left\{1 + \left[\frac{\bar{E}\,\bar{\varepsilon}}{\left(1 - \frac{\bar{E}'}{\bar{E}}\right)\sigma_{kink} + \bar{E}'\,\bar{\varepsilon}}\right]^{n+1}\frac{\bar{E}'}{\bar{E}}\right\}}{\left\{1 + \left[\frac{\bar{E}\,\bar{\varepsilon}}{\left(1 - \frac{\bar{E}}{\bar{E}}\right)\bar{\sigma}_{kink} + \bar{E}'\,\bar{\varepsilon}}\right]^{n}\right\}^{\frac{n+1}{n}}} \qquad (2.3.2)$$

To obtain equivalent plastic modulus H' for the multiaxial stress condition, which is the slope of effective stress vs. effective plastic strain curve, one may start from

$$d\bar{\varepsilon} = d\bar{\varepsilon}_e + d\bar{\varepsilon}_p \qquad (2.3.3)$$

Let

$$d\bar{\varepsilon}_p = \frac{d\bar{\sigma}}{H'} \quad , \qquad (2.3.4)$$

Since

$$d\bar{\varepsilon}_e = \frac{d\bar{\sigma}}{\bar{E}} \quad , \qquad (2.3.5)$$

$$d\bar{\varepsilon} = \frac{d\bar{\sigma}}{E_t} \quad , \qquad (2.3.6)$$

it follows that

$$H' = \frac{1}{\frac{1}{E_t} - \frac{1}{\bar{E}}} \quad . \qquad (2.3.7)$$

2.4 FINITE ELEMENT CONSTITUTIVE EQUATIONS

In the elastic-plastic problems, the application of the concept of incremental stationary potential energy leads to the incremental force-displacement equilibrium in each loading step:

$$\{ \Delta Q_i \} = [K_i] \{ \Delta u_i \} \qquad (2.4.1)$$

where i denotes the ith loading step.

The above relationship implies that the whole non-linear loading process now has been divided into many piecewise linear loading steps.

The key for elastic-plastic analysis is to get the elastic-plasticity matrix $[C_{ep}]$ which is different from the elasticity matrix $[C_e]$ in (1.1.3). Once the $[C_{ep}]$ matrix has been evaluated, the computation of nodal displacement increments, stress and strain increments can be carried out following the same procedures adopted in the elastic analysis.

It has been found that the plastic strain component increments are proportional to the current deviatoric stress components $\{ \sigma' \}$:

$$\frac{d\varepsilon_{11}}{\sigma_{11}'} = \frac{d\varepsilon_{22}}{\sigma_{22}'} = \frac{d\varepsilon_{33}}{\sigma_{33}'} = \frac{d\varepsilon_{13}}{\sigma_{13}'} = \cdots$$

which leads to the Prandtl-Reuse flow rule

$$\{ d\varepsilon_p \} = d\lambda \{ \sigma' \} \quad , \qquad (2.4.2)$$

where $d\lambda$ is a proportionality factor.

Referring to Eq.(2.2.2), it is found that

$$\sigma_{ij}' = \frac{\partial F}{\partial \sigma_{ij}} \quad , \qquad (2.4.3)$$

or in the matrix form:

$$\{ \sigma' \} = \{ \frac{\partial F}{\partial \sigma'} \} \quad . \qquad (2.4.4)$$

Now (2.4.2) becomes

$$\{ d\varepsilon_p \} = d\lambda \{ \frac{\partial F}{\partial \sigma'} \} \quad . \qquad (2.4.5)$$

If only the stress and the hardening parameter K are to be taken into account, (2.2.1) becomes

$$F = F (\{ \sigma \} , K) \quad , \qquad (2.4.6)$$

The differential form is

$$dF = \{ \frac{\partial F}{\partial \sigma} \}^T \{ d\sigma \} + \frac{\partial F}{\partial K} dK = 0 \quad . \qquad (2.4.7)$$

By expressing the hardening increment in terms of plastic strain, Eq.(2.4.7) can be expressed as follows

$$dF = \{ \frac{\partial F}{\partial \sigma} \}^T \{ d\sigma \} + \frac{\partial F}{\partial K} \{ \frac{\partial K}{\partial \varepsilon_p} \} \{ d\varepsilon_p \} = 0 \quad . \qquad (2.4.8)$$

The total increment of strain at any step is

$$\{ d\varepsilon \} = \{ d\varepsilon_e \} + \{ d\varepsilon_p \} \quad , \qquad (2.4.9)$$

in which $\{ d\varepsilon_p \}$ is the plastic strain increment and $\{ d\varepsilon_e \}$ is the elastic increment. From Hooke's law,

$$\{ d\varepsilon_e \} = [C_e]^{-1} \{ d\sigma \} \quad . \qquad (2.4.10)$$

Substitute (2.4.4) and (2.4.10) into (2.4.9), we have

$$\{ d\varepsilon \} = [C_e]^{-1} \{ d\sigma \} + d\lambda \{ \frac{\partial F}{\partial \sigma'} \} \quad , \qquad (2.4.11)$$

hence,

$$\{ d\sigma \} = [C_e] \{ d\varepsilon \} - [C_e] \{ \frac{\partial F}{\partial \sigma'} \} d\lambda \quad . \qquad (2.4.12)$$

Substitute (2.4.4) and (2.4.12) into (2.4.8) and solve for $d\lambda$,

$$d\lambda = \frac{\{ \frac{\partial F}{\partial \sigma} \}^T [C_e] \{ d\varepsilon \}}{\{ \frac{\partial F}{\partial \sigma} \}^T [C_e] \{ \sigma' \} - \frac{\partial F}{\partial K} \{ \frac{\partial K}{\partial \varepsilon_p} \}^T \{ \sigma' \}} \quad . \qquad (2.4.13)$$

The relation

$$\{ \frac{\partial F}{\partial \sigma'} \} = \{ \frac{\partial F}{\partial \sigma} \}$$

has been used in the above derivation.

Finally, combining (2.4.12) and (2.4.13) leads to:

$$\{ d\sigma \} = [C_e]\{ \Delta\varepsilon \} - \frac{[C_e] \{ \frac{\partial F}{\partial \sigma} \} \{ \frac{\partial F}{\partial \sigma} \}^T [C_e]}{S} \{ \Delta\varepsilon \} \quad , \quad (2.4.14)$$

where

$$S = \{ \frac{\partial F}{\partial \sigma} \}^T [C_e]\{ \frac{\partial F}{\partial \sigma} \} - \frac{\partial F}{\partial K} \{ \frac{\partial K}{\partial \varepsilon_p} \}^T \{ \frac{\partial F}{\partial \sigma} \} \qquad (2.4.15)$$

It is convenient to introduce the plasticity matrix:

$$[C_p] = \frac{[C_e] \{ \frac{\partial F}{\partial \sigma} \} \{ \frac{\partial F}{\partial \sigma} \}^T [C_e]}{S} \quad . \qquad (2.4.16)$$

and the elastic-plasticity matrix

$$[C_{ep}] = [C_e] - [C_p] \quad .$$

Up to now, a new constitutive relation has already been established for elastic-plastic analysis, which is

$$\{ d\sigma \} = [C_{ep}] \{ d\varepsilon \} \quad . \qquad (2.4.17)$$

It is also shown in [44] that

$$\left\{ \frac{\partial F}{\partial \sigma} \right\} = < \sigma'_{11}, \sigma'_{22}, 2\sigma'_{12} >^T \quad , \qquad (2.4.18)$$

$$\frac{\partial F}{\partial K} = -\frac{2}{3} H' \quad , \qquad (2.4.19)$$

$$\left\{ \frac{\partial K}{\partial \varepsilon_p} \right\} = \{ \sigma \}^T \quad , \qquad (2.4.20)$$

where H' is the plasticity modulus given in the previous section.

Since in the Plane stress case,

$$[C_e] = \frac{E}{1 - \nu^2} \begin{bmatrix} 1 & \nu & 0 \\ & 1 & 0 \\ \text{sym.} & & \frac{1 - \nu}{2} \end{bmatrix} \quad , \qquad (2.4.21)$$

we have

$$[C_e] \left\{ \frac{\partial F}{\partial \sigma} \right\}^T = \frac{E}{1 - \nu^2} \begin{Bmatrix} \sigma'_{11} + \nu \sigma'_{22} \\ \nu \sigma'_{11} + \sigma'_{22} \\ (1 - \nu) \sigma'_{12} \end{Bmatrix} \qquad (2.4.22)$$

and

$$[\,C_e\,]\,\{\,\frac{\partial F}{\partial \sigma}\,\}^T\,\{\,\frac{\partial F}{\partial \sigma}\,\}\,[\,C_e\,] \qquad (\,2.4.23\,)$$

$$= \frac{E}{(1-\nu^2)^2}\begin{bmatrix} (\sigma'_{11}+\nu\sigma'_{22})^2 & (\sigma'_{11}+\nu\sigma'_{22})(\nu\sigma'_{11}+\sigma'_{22}) & (1-\nu)\sigma'_{12}(\sigma'_{11}+\nu\sigma'_{22}) \\ & (\nu\sigma'_{11}+\sigma'_{22})^2 & (1-\nu)\sigma'_{12}(\nu\sigma'_{11}+\sigma'_{22}) \\ \text{sym.} & & (1-\nu)^2\sigma'^2_{12} \end{bmatrix}$$

Let

$$S_1 = \frac{E}{1-\nu^2}\,(\sigma'_{11} + \nu\,\sigma'_{22}) \quad ,$$

$$S_2 = \frac{E}{1-\nu^2}\,(\nu\,\sigma'_{11} + \sigma'_{22}) \quad , \qquad (\,2.4.24.\,)$$

$$S_3 = \frac{E}{1+\nu}\,\sigma'_{12} \quad ,$$

(2.4.23) becomes

$$[\,C_e\,]\,\{\,\frac{\partial F}{\partial \sigma}\,\}^T\,\{\,\frac{\partial F}{\partial \sigma}\,\}\,[\,C_e\,] = \begin{bmatrix} S_1^2 & S_1 S_2 & S_2 S_3 \\ & S_2^2 & S_2 S_3 \\ \text{sym.} & & S_3^2 \end{bmatrix}. \qquad (\,2.4.25\,)$$

On the other hand,

$$\left\{\frac{\partial F}{\partial \sigma}\right\}^T [\, C_e \,] \left\{\frac{\partial F}{\partial \sigma}\right\} = \sigma'_{11}\, S_1 + \sigma'_{22}\, S_2 + 2\, \sigma'_{12}\, S_3 \quad ,$$

$$\frac{\partial F}{\partial K} \left\{\frac{\partial K}{\partial \varepsilon_p}\right\}^T \left\{\frac{\partial F}{\partial \sigma}\right\} = -\frac{4}{9}\, \bar{\sigma}^{\,2}\, H' \quad , \qquad (2.4.26)$$

Substituting the above relationship into (2.4.15)

$$S = (\, \sigma'_{11}\, S_1 + \sigma'_{22}\, S_2 + 2\, \sigma'_{12}\, S_3 \,) + \frac{4}{9}\, \bar{\sigma}^{2}\, H' \quad . \qquad (2.4.27)$$

Finally,

$$[\, C_{ep} \,] = \frac{E}{1-\nu^2} \begin{bmatrix} 1 & \nu & 0 \\ & 1 & 0 \\ \text{sym.} & & \frac{1-\nu}{2} \end{bmatrix} - \frac{1}{S} \begin{bmatrix} S_1^2 & S_1 S_2 & S_1 S_3 \\ & S_2 & S_2 S_3 \\ \text{sym.} & & S_3^2 \end{bmatrix} \quad . \qquad (2.4.28)$$

Chapter III

CREEP DEFORMATION AND PSEUDO CREEP LOAD

3.1 REVIEW OF SOME BASIC CONCEPTS OF CREEP

The progressive deformation of a material at constant stress is called creep. Creep is a time-dependent phenomenon. A Creep curve is usually used to describe the strain change of a material vs. time at a certain temperature and a certain stress level. One way to get such a curve is to apply a constant stress to a tensile specimen maintained at a constant temperature and to measure the strain as a function of time.

A typical creep curve, curve A, is given in Fig.2. It is generally agreed that the creep curve has three stages. The first stage of creep, known as primary creep, represents a region of decreasing creep rate. The second stage of creep, known as secondary creep, is a period of nearly constant creep rate. For this reason, secondary creep is usually referred to as steady-state creep. The average creep rate in this stage is called the minimum creep rate which is the most important engineering design parameter.

The third stage or tertiary creep mainly occurs in constant load, high stress and high temperature tests. When low temperature and low stress tests are made, it is frequently

found that the second and the third stage will not occur and a creep curve like curve B in Fig.2 will be obtained.

At low temperatures, say, below half of the material's melting temperature, primary creep dominates. The commonly used creep law in this stage is

$$\bar{\varepsilon}^c = \beta\, t^p \qquad (3.1.1)$$

where $\bar{\varepsilon}^c$ is the effective creep strain, β and p are constants determined from experiments.

High-temperature creep is predominated by steady-state or viscous creep. The minimum creep rate is usually determined from "Norton's Law", which has the form

$$\dot{\bar{\varepsilon}}^c = K\, \bar{\sigma}^n\, e^{-Q/RT} \qquad (3.1.2)$$

where $\dot{\bar{\varepsilon}}^c$ = effective creep strain rate,

$\bar{\sigma}$ = effective stress,

Q = activation energy,

T = absolute temperature,

R = universal gas constant and

K, n = material constants.

3.2 ELASTIC-PLASTIC CONSTITUTIVE RELATIONS FOR CREEP ANALYSIS

Generally speaking, at any particular time, the strain rate of the structure is composed of

$$\{ \dot{\varepsilon} \} = \{ \dot{\varepsilon}^{*} \} + \{ \dot{\varepsilon}^{c} \} \qquad (3.2.1)$$

in which

$\{ \dot{\varepsilon}^{c} \}$ = the creep strain rate and

$$\{ \dot{\varepsilon}^{*} \} = \{ \dot{\varepsilon}_{ep} \} + \{ \dot{\varepsilon}_{T} \} + \{ \dot{\varepsilon}_{Te} \}$$

where $\{ \dot{\varepsilon}_{ep} \}$ = elastic-plastic strain rate,

$\{ \dot{\varepsilon}_{T} \}$ = thermal strain rate and

$\{ \dot{\varepsilon}_{Te} \}$ = strain rate due to temperature dependent material properties.

In our problem, the temperature is constant and (3.2.1) becomes

$$\{ \dot{\varepsilon} \} = \{ \dot{\varepsilon}_{ep} \} + \{ \dot{\varepsilon}^{c} \} \qquad (3.2.2)$$

where $\{ \dot{\varepsilon}_{ep} \}$ can be expressd by stress rate following the relationship given in (2.4.17):

$$\{ \dot{\varepsilon}_{ep} \} = [C_{ep}]^{-1} \{ \dot{\sigma} \} \qquad (3.2.3)$$

On the other hand, the creep strain rate can also be written in terms of a creep potential function [45]:

$$\{ \dot{\varepsilon}^c \} = \dot{\beta} \frac{\partial \psi (\{ \sigma \})}{\partial \{ \sigma \}} \qquad (3.2.4)$$

where $\dot{\beta}$ is a positive parameter depending on the loading history.

If the material is assumed to be homogeneous and isotropic with no Bauschinger effect, also to be incompressible and obeys Von Mises yield condition, the creep potential then takes the form of the second deviatoric stress invariant J_2 given in (2.2.3):

$$\frac{\partial \psi (\{ \sigma \})}{\partial \{ \sigma \}} = \frac{\partial J_2}{\partial \{ \sigma \}} = \{ \sigma' \} \qquad (3.2.5)$$

where $\{ \sigma' \}$ is the deviatoric stress components.

The creep strain rate tensor is related to the effective creep strain rate by

$$\bar{\dot{\varepsilon}}^c = (\frac{2}{3} \{ \dot{\varepsilon}^c \}^T \{ \dot{\varepsilon}^c \})^{\frac{1}{2}} \quad . \qquad (3.2.6)$$

Substitute (3.2.4) into (3.2.6) and solve for $\dot{\beta}$ one gets:

$$\dot{\beta} = \frac{3}{2} (\bar{\dot{\varepsilon}}^c / \bar{\sigma}) \quad . \qquad (3.2.7)$$

Substitute (3.2.5) and (3.2.7) into (3.2.4)

$$\{ \dot{\varepsilon}^c \} = \frac{3}{2} \left(\dot{\bar{\varepsilon}}^c / \bar{\sigma} \right) \{ \sigma' \} \quad , \qquad (3.2.8)$$

or

$$\{ d\varepsilon^c \} = \frac{3}{2} \left(d\bar{\varepsilon}^c / \bar{\sigma} \right) \{ \sigma' \} \quad . \qquad (3.2.9)$$

From (3.2.1), (3.2.3) and (3.2.4), the constitutive equation is obtained as

$$\{ \dot{\varepsilon} \} = [C_{ep}]^{-1} \{ \mathring{\sigma} \} + \frac{3}{2} \left(\dot{\bar{\varepsilon}}^c / \bar{\sigma} \right) \{ \sigma' \} \quad . \qquad (3.2.10)$$

3.3 FINITE ELEMENT FORMULAS

In Chapter 2, only mechanical load is considered. For creep analysis, however, a pseudo creep load has to be added on. The total load increment now is

$$\{ dF \} = \{ dP \} + \{ dP_c \} \qquad (3.3.1)$$

where $\{ dP \}$ is the mechanical load on the nodal points and $\{ dP_c \}$ is the pseudo creep load which takes the form

$$\{ dP_c \} = \int_v [B]^T [\sigma_c] dv$$
$$= \int_v [B]^T [C_{ep}] \{ d\varepsilon^c \} dv \quad . \qquad (3.3.2)$$

The equilibrium equation has the same form as (1.1.9)

$$[K] \{ du \} = \{ dF \} \qquad (3.3.3)$$

where [K] = elastic-plastic stiffness matrix and

{ du } = displacements of nodes in the finite element mesh.

Apply the load in (3.3.1) to the structure and solve (3.3.3), the displacement of every node may be calculated and the strain of every element may be obtained from

$$\{ d\varepsilon \} = [B] \{ du \} \quad . \qquad (3.3.4)$$

Also,

$$\{ d\sigma \} = [C_{ep}] \{ d\varepsilon_{ep} \} \quad ,$$

from which we get

$$\{ d\sigma \} = [C_{ep}] (\{ d\varepsilon \} - \{ d\varepsilon^c \}) \quad . \qquad (3.3.5)$$

3.4 INTEGRATION SCHEME

In this thesis, the Euler integration has been adopted as the numerical integration scheme to calculate the effective creep strain increment:

$$d\bar{\varepsilon}^{c} = \dot{\bar{\varepsilon}}^{c}\, dt \qquad (3.4.1)$$

where $\dot{\bar{\varepsilon}}^{c}$ is given by the Norton's Law.

In the elastic-plastic analysis, the magnitude of the load increment has to be controlled so that the accumulated error will not be too high. In creep problems, selection of the time increments becomes very important. Too large a time step can lead to unacceptable errors or even divergence of the solution. Cormeau and Irons et al [46] suggested that the integration can be made if the ratio of the maximum creep strain increment and the elastic strain at that point is kept below 2/n where n is the exponent of the Norton's Law. From that, a maximum time increment Δt_m for power-law creep has been given in [47] in terms of the maximum effective stress $\bar{\sigma}_{max}$:

$$\Delta t_m = \frac{4\,(1+\nu)}{3\,n} \frac{(\bar{\sigma}_{max} / E)}{K_c\, f(T)\, (\bar{\sigma}_{max})^{n}} \quad . \qquad (3.4.2)$$

Although (3.4.2) is derived for elastic creep analysis, it is easy to understand that it can be applied to elastic-plastic creep analysis due to the fact that the elastic strain would be small in comparison to the total strain which is the sum of the elastic and the plastic strain.

Chapter IV

FRACTURE MECHANICS IN DUCTILE MATERIALS

4.1 INTRODUCTION

Since fracture mechanics was introduced as a result of the study of brittle fractures of steel at low temperature, more attention was paid to linear or elastic fracture analysis in early studies of this subject. The theory of linear fracture mechanics is well established. This thesis deals only with the fracture of ductile solids. No attempt was made here to retroact the elastic fracture theory and a review of ductile fracture is presented in this chapter.

4.2 THE SHAPE OF THE PLASTIC ZONE

The elastic stress functions at the crack tip in a polar coordinate system are

$$\sigma_1 = \frac{K}{\sqrt{2\pi r}} \cos\frac{\theta}{2}\left(1 + \sin\frac{\theta}{2}\right)$$

$$\sigma_2 = \frac{K}{\sqrt{2\pi r}} \cos\frac{\theta}{2}\left(1 + \sin\frac{\theta}{2}\right)$$

$$\sigma_3 = \nu(\sigma_1 + \sigma_2) = 2\nu\frac{K}{\sqrt{2\pi r}}\cos\frac{\theta}{2} \qquad \text{for plane strain,}$$

$$\sigma_3 = 0 \qquad \text{for plane stress}$$

where K is the stress intensity factor, r is the vector distance from the crack tip, θ is the angle between the vector and the X-axis (Fig.8), σ_1 , σ_2 and σ_3 are the principal stresses, the principal stresses σ_1 and σ_2 are equal and act in x and y directions on the plane $\theta = 0$.

Substitute these equations into the Von Mises yield condition which gives the yield surface of a material under a certain stress condition

$$(\sigma_1 - \sigma_2)^2 + (\sigma_2 - \sigma_3)^2 + (\sigma_3 - \sigma_1)^2 = 2 \sigma_{ys}^2$$

where σ_{ys} is the yield stress, and solve r as a function of θ, the boundary of the plastic zone is obtained as :

$$\text{Plane strain: } r (\theta) = \frac{K^2}{4 \pi \sigma_{ys}^2} [\frac{3}{2} \sin^2\theta + (1 - 2 \nu)^2 (1 + \cos \theta)] \qquad (4.2.1)$$

$$\text{Plane stress: } r (\theta) = \frac{K^2}{4 \pi \sigma_{ys}^2} [1 + \frac{3}{2} \sin^2 \theta + \cos \theta] \qquad (4.2.2)$$

A non-dimensional $r^* = r / (K / \pi \sigma_{ys})^2$ vs. θ curve is plotted in Fig.3 a. The region inside this curve is the plastic zone.

There is another plastic zone shape function derived from the Tresca yield criterion:

plane stress: $$r = \frac{K^2}{2\pi\sigma_{ys}^2}\left[\cos\frac{\theta}{2}\left(1+\sin\frac{\theta}{2}\right)\right]^2 \quad , \qquad (4.2.3)$$

plane strain:

$$r = \frac{K^2}{2\pi\sigma_{ys}^2}\cos^2\frac{\theta}{2}\left[1-2\nu+\sin\frac{\theta}{2}\right]^2 \quad \text{or} \quad r = \frac{K^2}{2\pi\sigma_{ys}^2}\cos^2\frac{\theta}{2}$$

whichever is larger. (4.2.4)

The corresponding figures are in Fig.3 B.

Tuba [49] and Rice and Rosengren [50] did more accurate analysis on this problem by using relaxation methods. The results are presented in Fig.4. Tuba's result showed that the line connecting the farthest point of the plastic boundary and the crack tip is at an angle $\theta = 69^\circ$ from the crack line. Note that this is almost the angle at which maximum shear stress occurs. Rice and Rosengren however calculated an angle of 100°.

All these analytical results need experimental verification. The dark area in Fig.5 A [51] shows a plastic zone in plane stress which resembles Tuba's modal well and Fig.5 B [40] is another example which confirms Tuba's model to be a more realistic one.

4.3 PLASTIC ZONE CORRECTION METHOD

Since most engineering materials have the ability to deform plastically, the elastic solutions of crack problems cannot be applied directly. However, it would be easier to solve the elastic-plastic problems by correlating plastic fracture to the existing elastic theories. Irwin [51,52] and Dugdale [53,54] proposed two different plastic zone correction methods to approximate an elastic-plastic fracture solution to an elastic fracture problem.

It is a condition in both of these therories that the occurrence of plasticity makes the crack behave as if it were longer than its physical size as the existence of plasticity increases the displacement and decreases the stiffness of the plate specimen.

They assumed that

$$a = a_0 + \delta \qquad (4.3.1)$$

where a is the equivalent crack length, a_0 the physical length of the crack and δ is the additional length to be calculated as follows:

According to Irwin,

$$\delta = \frac{1}{2\pi} \frac{K^2}{\sigma_{ys}^2} \qquad (4.3.2)$$

for plane stress case.

From Dugdale:

$$\frac{a_0}{a_0 + 2\delta} = \cos\frac{\pi\sigma}{2\sigma_{ys}} \qquad (4.3.3)$$

where σ is the gross section stress.

For small value of σ / σ_{ys}, δ is obtained from (4.3.3) by the series development of the cosine,

$$\delta = \frac{\pi}{16}\frac{K^2}{\sigma_{ys}^2} \quad . \qquad (4.3.4)$$

In this case, the two methods lead to similar solutions because (4.3.2) and (4.3.4) are almost identical. For large values of σ / σ_{ys}, the difference between these two methods become significant because (4.3.3) should be used instead of (4.3.4) by Dugdale's method.

The application of this method is limited by the fact that when the plastic zone size is too small in comparison to the crack size, this correction might be unnecessary. however, when the plastic zone size becomes large, the validity of this method becomes questionable as we will realize that the stress intensity factor K which is involved in all the three expressions of δ is derived from the theory of elasticity.

4.4 THE ENERGY PRINCIPLE

4.4.1 The Crack Growth Resistance (R Curve) Method

The crack growth resistance of a ductile solid can be defined as:

$$R = \frac{dW}{da}$$

where W is the energy required for the crack growth.

As the crack growth resistance R represents the energy required for crack growth, R is considered independent of crack length under plane strain or brittle fracture conditions. In the case of plane stress or ductile fracture, the crack resistance varies with the amount of crack growth.

Fig.6 shows a typical R curve and its physical meaning. The straight lines represent the stress intensity factors $K = \sigma \sqrt{\pi a}$ vs. crack length a.

When the R curve starts from zero, the material at the crack tip is not ready to separate until the stress increased to σ_0 where the corresponding K_0 intersects the R curve at $a = a_0$ and crack growth takes place. After the crack grows to a_1, the K line intersected with R curve becomes K_1 which corresponds to a higher stress level σ_1. If the applied stress remains at σ_0 the crack growth will stop. The crack growth can be resumed only when the stress is increased to a higher level, i.e. σ_1. Physically it

means that as the crack grows longer, the resistance of the material to arrest the crack growth tends to increase, in other words, the energy required to maintain the crack growth becomes larger. The increased energy is mainly the additional work to form a new and larger plastic zone to overcome the increased strain hardening ahead the crack tip as the crack advances.

Note that the K line is tangent to the R curve at a = a_2. After the crack length reaches a_2, the rate of supplied energy will be always higher than the rate of the resistant energy so a_2 is the critical point where unstable crack propagation occurs.

The R curve might be invariant with the initial crack size as pointed by Krafft et al [55]. An energy criterion for fracture mechanics provided by the R curve is possible if an analytical expression for R curve can be derived. However, the theory of the R curve is still under development.

4.4.2 The J-Integral

Another energy method was proposed by Rice [56] which is the J-integral method. J-integral is a line integral with the form

$$J = \int_{\Gamma} \left(W \, dy - T \frac{\partial u}{\partial x} \, ds \right)$$

where Γ = a contour surrounding an area at the crack tip (refer to Fig.7)

T = the tension vector perpendicular to Γ ,

u = the displacement in x direction,

ds = an increment length on Γ and

W = the strain energy per unit volume.

For elastic fracture or small scale yielding, the physical meaning of J-integral was explained by Rice [57] to be:

$$J = - \frac{\partial U}{\partial a}$$

where U is the potential energy which gives a generalized relation for the energy release due to crack propagation. Since the J-integral value has been proved to be path independent for small strain case [56], one may select a most convenient path to perform the integration. It may be expected that there is a critical value at which crack growth will occur. Begley and Landes [58,59] found that fracture indeed occurs at a constant J_{IC} .

The J-integral seems to be a better description for cases with some plasticity but it is limited to characterize the initiation of a crack or some limited crack growth because one of the preliminaries in proving the path independence is the deformation theory of plasticity which does not allow for localized unloading phenomenon which takes place behind the crack tip during a stable crack growth process.

4.5 THE CRACK OPENING DISPLACEMENT CRITERION

When the net section stress beyond the yield stress which is defined to be:

$$\sigma_{net} = \sigma \frac{w}{w - a} \geqslant \sigma_{ys} \quad ,$$

in which w is the width of the specimen, the plastic zone becomes very large and it may spread through the entire cracked section. This is called general yielding. Under this condition, a measure for the plastic strain at the crack tip can be made by the crack tip opening displacement CTOD. The CTOD criterion was first proposed by Wells [60,61].

Following the Dugdale approach, CTOD can be calculated to give:

$$CTOD = \frac{8 \sigma_{ys} a}{\pi E} \log \sec \frac{\pi \sigma}{2 \sigma_{ys}} \quad . \qquad (4.5.1)$$

Again, for the case of small σ / σ_{ys} , (4.5.1) reduces to

$$\sigma = \frac{K^2}{\sigma_{ys} E} \quad . \qquad (4.5.2)$$

Although CTOD cannot provide a quantitative solution to the fracture problem, it shows one possible way to extend fracture mechanics to highly ductile materials, it can also indicate the toughness of a material to fracture. A general rule is that the higher the CTOD value, the better the crack resistance.

Chapter 5

SIMULATION OF THE CREEP CRACK GROWTH

5.1 DESCRIPTION OF THE PROBLEM

A center notched plate under consideration is depicted in Fig.8. This plate had the same dimensions as the center notched plate described in Ohtani's paper [40] for the creep test which was conducted at a constant load in a single lever creep tester. The plate was 32 mm wide, 50 mm long and 2.3 mm thick. A 5 mm long initial crack was situated at the center of the plate. Since the plate was very thin in comparison to the width, plane stress finite element formulae were used in this analysis.

The material of this plate was assumed to be 304 stainless steel. Table 1 presents the mechanical properties of this material used in the analysis. It should however be noted that there is considerable variable in these properties as listed in different handbooks. The values listed in table 1 represent a reasonable estimate of these values.

The gross section stress level was 98.1 MPa but for the case of ε_f = 12% a higher level of 135 MPa was also applied. The environmental temperature was maintained at 650°C for all cases. According to the discussion before, under such a high temperature, the secondary or steady-state creep dominates. By neglecting the effect of the activation energy, the Norton's creep Law becomes:

$$\dot{\bar{\varepsilon}}^{c} = K_c \left(\bar{\sigma} \right)^n$$

where $\bar{\sigma}$ has the dimensions of MPa, the respective values of K and n for the material at 650°C are 1.37×10^{-17} and 7.1.

All case studies presented here are limited to mode I type of crack growth.

5.2 FINITE ELEMENT MESH

Special isoparametric elements, special triangular elements and circular elements have been used in elastic stress analysis around a crack tip which can simulate the singularity of the stress at the crack tip and showed great advantage by obtaining the same result with fewer elements. However, in the elastic-plastic analysis, simple but smaller elements have been used for computational simplicity and accuracy.

In the present analysis, only a quarter (the shaded part in Fig.8) of the plate was taken into consideration due to symmetry of the geometry. This quarter was divided into a mixture of quadrilateral and triangular elements as shown in Fig.9. Around the crack tip, the elements needed to be very small for large stress strain gradients in that region. As the distance from the crack tip increases, the elements became larger and larger. Fig.9 A shows the finite element meshes for the whole quarter plate and Fig.9 B gives the detail of region A in Fig.9 A. The ratio of the length of the elements near the crack tip and the original crack length was 0.2/2.5 = 0.08. A total of 325 elements and 232 nodes were used.

It is obvious that there must be some limitation on the element size. Beyond it, the problem might not converge. An attempt was made to find a suitable compromise. The conclusion is that this model is good enough for this particular problem.

5.3 CRITERION OF CRACK PROPAGATION

In elastic fracture mechanics, it is considered that crack extension will occur when the stress intensity factor K reaches a critical value K_c, the fracture toughness of the material. In the elastic-plastic fracture analysis, critical values of COD, J-integral, the ultimate tensile strength and the rupture strain criterion etc have been suggested as fracture criteria. Let us just focus our attention on the rupture strain criterion for the time being.

There were a few researchers [62,63,64] who attempted to measure the strain field around the crack tip. They found that the strain around the crack tip was almost a constant during the fracture process. The rupture strain criterion states that when the state of the strain at the crack tip reaches a certain value fracture will occur [65].

There should be only one rupture strain for one material under certain mechanical and environmental conditions during elastic-plastic deformation, which can be obtained through experiments. This criterion appeared to work satisfactorily in [69,70]. However, it is not clear at this point whether a

single value of rupture strain can describe the entire creep stage. The purpose then of this thesis is not to determine all the parameters in creep fracture analysis quantitatively, but rather to use three arbitary rupture strain 0.03, 0.075 and 0.12 and to assess their sensitivity to the crack growth behaviour.

5.4 THE CONCEPT OF THE "BREAKABLE ELEMENT"

In the present analysis, the crack was considered to extend in a predetermined crack growth path. Those elements along x-axis from the crack tip in Fig.9 B were assumed to be "breakable". the following sections describe how they broke gradually one after another [69,70].

5.4.1 Extrapolated Strain

Since the present analysis is based on the basic principle used in the TEPSA computer code on the constant stress strain elements, the effective strains in the breakable elements could be extrapolated as a smooth curve towards the crack tip by a least squares curve fitting technique [66]. It was found that usually the strains changes abruptly from the first to the fourth element, so the variation of the effective strain in the first four elements ahead of the crack tip had been considered. A polynomial function was used to describe such a variation:

$$\bar{\varepsilon}\,(x) = a_1 x^3 + a_2 x^2 + a_3 x + a_4 \qquad (5.4.1)$$

where x denotes the distance from the crack tip along the crack path, a_1, a_2, a_3, a_4 are constants derived from the least squares analysis by using the average strains at the element centroids (x_1, x_2, x_3, x_4).

The extrapolated strain at the crack tip can be expressed as:

$$\bar{\varepsilon}_{ext} = \bar{\varepsilon}\,(0.) \quad .$$

5.4.2 Rupture of Breakable Elements

At first, $\bar{\varepsilon}_{ext}$ was smaller than ε_{rup} or ε_f, the rupture strain. As the creep deformation increases, $\bar{\varepsilon}_{ext}$ would eventually exceed ε_f, at such time the crack growth process began. The amount of crack extension Δx was evaluated by solving for x in Eq.(5.4.1) with $\bar{\varepsilon}\,(x) = \varepsilon_f$. It can be illustrated schematically in Fig.10 as the crack growth at time step i.

At time step i+1, due to the creep deformation, the strain in the crack tip element would have increased further and the strain at point a might exceed ε_f. The same procedure like in time step i would be repeated again as

illustrated in Fig.11. This process went on and on until point a reached the next node.

5.4.3 Force Relaxation of the Broken Element

In Chapter 2, the equilibrium equation was shown to be

$$\begin{aligned} \{ F \} &= K \{ u \} \\ &= \int_V [B]^T [C] [B] \, dv \{ u \} \\ &= \int_V [B]^T [C] [B] \{ u \} \, dv \end{aligned} \qquad (5.4.2)$$

from above, the nodal force components are:

$$\begin{aligned} \{ F \} &= \int_V [B]^T [C] \{ \varepsilon \} \, dv \\ &= \int_V [B]^T \{ \sigma \} \, dv \end{aligned} \qquad (5.4.3)$$

Once the crack front had passed through a crack tip element, this element was deemed to have fractured and became incapable of carrying any load. The nodal forces carried by this element before it broke had to be released to redistribute the stress field of the plate. This force release is called relaxation step in this analysis.

In the relaxation step, the stiffness matrix of the broken element was reduced to zero so it could not carry any load in the later analysis.

Since the restrictions on nodes 1 & 2 were all normal to the crack, only reaction forces in this direction would be given back to the structure as illustrated in Fig.12. In order to maintain a smooth computation, small load increment had to be used. The reaction forces were divided by 15 segments and were added on the structure by 15 pseudo-time steps. A stress analysis was performed with these nodal forces while the external load remained unchanged.

During the relaxation process, some elements would be kept under loading while others would be under unloading in these elements around the newly created free crack surfaces.

Loading or unloading of the elements was determined by a trial and error technique. In trial step 1, all elements were assumed to be under loading. Eq.(1.1.9) was solved and the incremental stresses were added on in the usual way. The effective stress $\bar{\sigma}$ of each element obtained in the trial load step would be compared with the effective stress prior to the trial step. According to $\bar{\sigma}_2 \geq \bar{\sigma}_1$ or $\bar{\sigma}_2 < \bar{\sigma}_1$, the loading and unloading elements was determined respectively (Fig.13). The stress prior to the trial step was then restored, the analysis of trial step 2 with the stiffness matrices of those yielded unloading elements changed from $[\ C_{ep}\ ]$ to $[\ C_{e}\ ]$ was carried out.

Chapter VI

PROGRAM AND SOLUTION PROCEDURE

6.1 INTRODUCTION

The program TEPSA [43] was used as the basis for the present analysis. It was originally developed by Prof. Hsu and his associate, A.A.M. Bertels to handle thermal elastic plastic stress problems. The crack propagation part has been implemented by Y.J. Kim and the creep analysis part by Y.J. Liu. The author combined all these elements together to make a new program which can now deal with creep crack growth problem.

The procedure of this program work is as follows:

6.2 MECHANICAL LOADING

The load increment for the first step was 21 MPa which was almost the maximum value to keep the structure in fully elastic. Subsequent load increments of 1 MPa, 0.5 MPa and 0.25 MPa were used as the load increases. To reach the gross section stress levels at 98.1 MPa and 135 MPa, 120 and 180 steps were used correspondingly.

In order to simplify the analysis, creep effect was not considered in the initial mechanical loading as this effect may be neglected for short time duration involved.

The elastic-plastic stress analysis in the initial loading stage was performed according to the following steps:

1) Compare for each element the present effective stress with the yield stress, if $\bar{\sigma} < \sigma_y$, form the elasticity matrix [C_e]. If $\bar{\sigma} \geq \sigma_y$, form the elastic-plastic matrix [C_{ep}]. Form element stiffness matrices [K_e] and the overall stiffness matrix [K].

2) Evaluate the mechanical load matrix { F } on every node of the structure.

3) Solve for { du } from the following equations:

$$[K] \{ du \} = \{ dF \} \qquad (6.1)$$

then calculate the strain and stress from

$$\{ d\varepsilon \} = [B] \{ du \} \qquad (6.2)$$

and

$$\{ d\sigma \} = [C_e] \{ d\varepsilon \} \qquad (6.3)$$

for elastic deformation, or

$$\{ d\sigma \} = [C_{ep}] \{ d\varepsilon \} \qquad (6.4)$$

for the elastic-plastic deformation.

4) Add this stress increment to update the stress

$$\{ \sigma_{i+1} \} = \{ \sigma_i \} + \{ d\sigma \} \quad .$$

5) Update new coordinates of nodes

$$\{ x \}_{i+1} = \{ x \}_i + \{ du \} \quad .$$

6) Repeat from step 1 with the newly defined coordinates.

6.3 CREEP ANALYSIS

Creep analysis started right after the initial mechanical loading finished. The procedure is as follows:

1) Find the element possessing the maximum effective stress from all the elements.

2) Use the maximum effective stress to compute Δt in (3.4.2) and $\dot{\bar{\varepsilon}}^c$ in (3.1.2).

3) Determine $d\bar{\varepsilon}^c$ from Eq.(3.4.1) where Δt and $\dot{\bar{\varepsilon}}^c$ has been evaluated in step 2 and $\{ \dot{\varepsilon} \}$ from (3.2.10) and also $\{ dP_c \}$ from (3.3.2).

4) Forward to the next time step i+1 with the pseudo creep load $\{ dP_c \}$ and perform the elastic-plastic analysis for the whole structure again.

5) Evaluate the total strain increment $\{ d\varepsilon \}$ by using (6.1) with the specified value of $\{ du \}$ in step 4 and the stress increment $\{ d\sigma \}$ from (3.3.5).

6) Use (6.5) to update the nodal coordinates and (6.4) to update the stress.

7) Repeat from step 1 again.

6.4 CRACK PROPAGATION

Creep is a time dependent phenomenon. Therefore as the time passed, the strains in every element of the structure graw until the extrapolated strain at the crack tip reached the critical value and then crack growth started. This procedure has already been described in Chapter 5 so it will not be repeated here. It is worth noting that after the relaxation step of a broken element, the extrapolated strain at the new crack tip might not yet reach the rupture strain. The creep analysis would then continue until $\bar{\varepsilon}_{ext} \geq \varepsilon_f$.

As time increased the "breakable" elements ruptured one after another until the crack propagation became unstable.

Chapter VII

RESULTS AND DISCUSSION

7.1 CRACK GROWTH RATE VS. TIME CURVES

The extrapolated strain at the tip of the crack was 0.015 at the completion of the mechanical loading at 98.1 MPa. After a creep relaxation of 1.6 hours, it reached a rupture strain of 0.03 then crack propagation initiated. In Fig.14, curve A represent the crack length vs. time for ε_f = 0.03, curve B for ε_f = 0.075 and curve C for ε_f = 0.12. The elapsed time before crack initiation were 10.5 hours and 28.8 hours for ε_f = 0.075 and 0.12 correspondingly.

The curves in Fig.15 represent crack growth rates $\dot{a}$ vs. time for the three cases under the same gross stress level of 98.1 MPa.

These two figures indicate that as the assigned rupture strain increases, both the crack growth and the rate of crack growth decreases and the crack growth initiation is delayed as well.

Actually, in many creep tests for ss 304 at 650°c, the elongation exceeds 60% which suggests a much higher rupture strain than the present 12%. However, computing condition limits the analysis to include a rupture strain of o.5 or o.6. By varying the rupture strain from 0.03 to 0.12, a

trend indicates that the crack growth rate can approach the experimental value of 0.001 mm/hr obtained through experiments [12] (0.152 for ε_f = 0.03, 0.441 for ε_f = 0.075 and 0.0242 for ε_f = 0.12) when ε_f approches say 0.5.

7.2 SHAPE AND SIZE OF THE PLASTIC ZONE

The shape of the plastic zone formed during loading process for the case of ε_f = 0.03 is shown in Fig.16. It coincides with some experimental works described in Chapter 4 and also some finite element stress analysis results [67,68]. It indicates that the present finite element analysis is adequate in simulating the crack propagation process during creep deformation.

The case study started from the stress level of 98.1 MPa which corresponds to the smallest plastic zone in Fig.16. However, by the time the extrapolated strain reached the rupture strain of 0.03, the plastic zone diminished to within only a few elements due to the creep stress relaxation. This was also true for the cases of ε_f = 0.075 and 0.12.

During the crack opening process, the variations of the plastic zone were different for three cases. For ε_f = 0.03, the plastic zone enlarged as the crack advances till the last element was broken. By then, the plastic zone was almost restored to the size at the end of initial mechanical loading at 98.1 MPa as shown in Fig.16. This process is illustrated schematically in Fig.17.

As for the cases of ε_f = 0.075 and 0.12, the crack growth rates were so low that it provided ample time for the creep relaxation to take place and hence the stress concerntration at the crack tip became less phenomenal. Consequently, the plastic zone did not expand as much as in the case of ε_f = 0.03. As a matter of fact the very small plastic zone remained unchanged all the way to the end of the computation.

There is one thing which has to be clarified. Consider the case of gross section stress level of 135 MPa. At the end of this initial loading, an extrapolated strain of 0.104 was obtained. This is much larger than 0.015 resulting from the case of gross section level of 98.1 MPa. The excessive strain of our incremental method is questionable. Fortunately, this problem of excessive strain has already been recognized and therefore a case study with a gross section stress level of 135 MPa and a rupture strain of 0.12 has been treated as a trial case and is good only for comparison.

7.3 STRESS AND STRAIN DISTRIBUTIONS

The effective stress distribution ahead of the crack tip at different stages of crack propagation is presented in Fig.18 where A, B and C correspond to the assigned strains of 0.03, 0.075 and 0.12 under the same stress level of 98.1 MPa. In each figure, the first curve is drawn at the crack initiation, the second curve is after the first element "broken" and so on.

These curves are not as smooth as those obtained by Taira and Ohtani [12] and Kim [69] due of the difference of assumptions. In Taira and Ohtani's case, the material was assumed to be elastic and visco-elastic therefore the stress rising towards the crack tip was very high. In Kim's case, the gradient was also high because the elastic-plastic materials were considered to be at room temperature with very high yield stress. In the present case there is a higher temperature and a lower yield stress than in Kim's case.

In this analysis, a low yield stress and a low gross stress level made the stress distribution curve relatively gradual hence the stress distribution tended to be sensitive to the nodal relaxation forces. This is proved by Fig.19 which is the stress distribition ahead of the crack during crack growth process with the initial gross stress level at 135 MPa in which the stress gradient is greater but the variation is more smooth than that in the case of 98.1 MPa gross section stress.

Some other features of the stress curves are: The crack tip stress keeps rising although the variations become less drastic as the crack grows. The distribution curves become fairly smooth beyond a certain distance from the original crack tip position.

The stress normal to the crack line is termed σ_{yy}. This stress and σ_{xx} component and the shear stress σ_{xy} are also plotted in Fig.20. For each case, three curves are drawn: 1. crack growth initiation, 2. after the fourth element broken and 3. after the last element broken.

The shape of σ_{xx} and σ_{yy} curves are similar to the effective stress $\bar{\sigma}$ except the magnitudes are all smaller. The σ_{xx} and σ_{yy} for the three cases ε_f = 0.03, 0.075 and 0.12 at the same stage of crack growth are close but the shape of σ_{xy} does vary abruptly. Having noticed that the magnitudes of σ_{xy} are all small (less than 25 MPa), these fluctuations are most likely caused by the numerical errors and hence present no serious concern.

The effective strains are very nicely distributed in front of the crack tip as illustrated in Fig.21. Variation of peak strains at various stages of crack growth have been observed. At ε_f = 0.03, the strain decreases very fast from the crack tip till the fifth element or a distance of 1.0 mm from the crack tip. This trend has slowed down significantly afterwords whereas for the case of ε_f = 0.12, the strain keeps decreasing but not as fast as in the previous case until a distance of 2.4 mm, which is 2.4 times of the distance in the case of ε_f = 0.03. Note that these two figures are under the same stress level. It is again creep which is responsible for this phenomenon.

7.4 CRACK PROFILE AND CRACK OPENING ANGLE

As has been discussed in Section 7.2, under the same stress level of 98.1 MPa, the crack opening would take place in a larger plastic state for the case ε_f = 0.03 than for the other two cases. This leads to a blunted crack profile

in Fig.22 A for ε_f = 0.03. Within the three figures of Fig.22, A is closer to that produced by Kim [67] and C is closer to Taira's results [12]. The reason is that the structure tends to be less plastic and hence less ductile in case c with ε_f = 0.12.

The other two parameters which are sometimes used in fracture mechanics are COA (Crack Opening Angle) and CTOA (Crack Tip Opening Angle). COA is the value of the crack opening displacement increment divided by the crack increment and CTOA is the angle of crack opening at the crack tip.

Fig.23 and Fig.24 show the COA and CTOA with respect to the position of the advancing crack tip, from which one may observe that COA tends to decrease as crack advances, which is also observed in [69], and CTOA fluctuates significantly with higher rupture strain values.

In elastic-plastic stress analysis, CTOA can be used as a fracture criterion as these values are almost constant during crack propagation such as shown in [69,73]. In the case of creep crack propagation, CTOA might not be a good fracture criterion to use as such consistency is no longer observed.

7.5 THE C* PARAMETER IN CREEP CRACK GROWTH

Based on the concept of the J-integral, Landes and Begley [18] proposed the C* parameter defined as:

$$C^* = \int_\Gamma W^* \, dy - T \left(\frac{\partial \dot{u}}{\partial x} \right) ds \qquad (7.5.1)$$

where the integral contour and other symbols are the same as for the J-integral except

$\dot{u}$ = the displacement rate and

$$W^* = \int_0^{\dot{\varepsilon}_{mn}} \sigma_{ij} \, d\varepsilon_{ij} \, .$$

C* was proposed for elastic-viscoelastic materials or materials which exhibit small scale yielding like the J-integral, it has the energy rate interpretation only under these conditions. Some formulae for evaluating C* were derived, among them, the simplest one was given by Ohji and his coworkers in 1978 [71] which has the form:

$$C^* = \frac{n - 1}{n + 1} \sigma_{net} \dot{v} \qquad (7.5.2)$$

where n = the exponent of Norton's creep law,

σ_{net} = the net section stress and

$\dot{v}$ = crack opening displacement rate.

Ohtani [40] compared the C* value calculated by this formula and the one by the integration through finite element analysis and found that the value given by this formula is about fifteen percent smaller than the finite element solution. Hsu, Liu and Zhai [72] also studied the corelation of the C* from (7.5.1) and (7.5.2) and found that the C* value by (7.5.2) was far from (7.5.1) but very close to C_g^* which was proposed by Liu and Hsu [29]. Note that C_g^* includes a plastic energy rate integral term. From this, the value of C* from (7.5.2) might represent a modified C* which can be used for materials with larger plasticity instead of the original C* defined in elastic analysis for materials with very small plasticity. Eq.(7.5.2) was chosen for this analysis to evaluate the C* parameter.

After every element was broken, C* and the crack growth rate $\dot{a}$ were calculated. The three short curves in Fig.25 were obtained after all the eight elements were broken.

Up to now, most $\dot{a}$ vs. C* relations were established through experiments. In Taira and Ohtani's analytical work, this problem was touched by merely given a group of straight lines of dimensionless crack growth rate with respect to dimensionless C* with no furhter discussion. It will be explored in a little detail in this research work.

The long straight line in Fig.25 is the experimental result for 304 stainless steel at 650°c [40]. At a stress level of 98.1 MPa, the experimantal data can be connected to be a curve on that line as shown. It is easily observed that

the three calculated curves are almost parallel to the experimental curve. It looks as if the curve for $\varepsilon_f = 0.03$ is shifting down towards the experimental curve as the rupture strain approaching a more realistic value ---- 0.5 or 0.6. It can be concluded that the analytical comparison to the experimental result from the present numerical analysis is quite possible.

Another group of curves in Fig.26 will further reinforce the above assessment in a different way. The rupture strains for these three hypothetical curves are 0.03, 0.075 and 0.12 respectively but the gross stress levels have been modified to 98.1 MPa, 110 MPa and 135 MPa correspondingly. These three curves can be shifted horizontally toward the experimental curve.

Another characteristic of these curves in Fig.26 is that there is a point at which the $\dot{a}$ vs. C* curve changes its slope to unity. This phenomenon was also observed by Landes and Begley [18]. They found that the point of the slowest crack growth rate lied far below the line through the other test points. A threshold value of C* similar to the threshold K for the fatigue crack growth rate control parameter was thus postulated. Physically, it means that below this threshold, the crack will not start to grow. Indeed, if one takes a closer look at the two curves for $\varepsilon_f = 0.075$ and $\varepsilon_f = 0.12$ in Fig.26, which correspond to higher stress levels of 110 MPa and 135 MPa and hence have

higher crack growth rate, the threshold point vanishes in both these cases. Further investigations on this problem is necessary in the future by both experimental and analytical investigations.

The slope of the third curve in Fig.26 needs some explanation as well. This curve is for the rupture strain 0.12 and gross stress level 135 MPa . The mathematical relationship between the crack growth rate and C* parameter established through this curve is

$$\dot{a} = 0.050 \ (C^*)^{1.155}$$

which deviates from linear relationships as have been presented by experimentalists. As discussed earlier, the extrapolated strain under gross section stress level of 135 MPa is fairly large to introduce significant error when using small strain theory such as in the present analysis.

7.6 COMPUTER EXECUTING TIME

The computer executing time was approximately 5 hours for the case of a rupture strain of 0.03 and 10 hours for the case of a rupture strain of o.12 respectively. A restart capability made this time consuming computing possible for this analysis.

Chapter VIII

CONCLUSIONS AND RECOMMENDATIONS

A new numerical method for creep crack propagation analysis has been proposed. This method is powerful by its general considerations of elastic-plastic creep behaviour of materials. The adoption of "breakable element" and "relaxation" of a broken element allows unloading of the material behind the crack tip to occur immediately after the crack tip element breaks.

The results showed in Chapter 7 have illustrated the applicability of this method and the established computer program. It is hoped that this method and program can be used to study the relationship between $\dot{a}$ and C* and C_g^* for structures with complex geometries. The conclusions and recommendations are as follows:

1) Due to the effect of creep, the stress at the crack tip decreased and the strain at the crack tip increased steadily as the time elapsed in the creep fracture process. Besides, the stress distribution in front of crack tip tended to be very sensitive to the crack propagation while the strain was not as sensitive . The rupture strain criterion is therefore considered to be more suitable for creep crack problem.

2) The crack opening angle and the crack tip opening angle both showed some gradual fluctuations which is unlike the elastic-plastic situations.

3) Beyond a certain value of the creep crack growth rate $\mathring{a}$, $\mathring{a}$ can be related to the C* parameter by a linear relation.

4) Further study of C* and C_g^* parameters for their usage and limitations in creep fracture mechanics is warranted.

5) Well planned and executed experiments are necessary to obtain the material properties such as: rupture strain, yield stress, tangent modulus and the multi-dimensional creep law with unloading behaviour etc. Experimental verifications of the analytical results produced by the present method are also required so that a quantitative numerical analysis can be established.

6) Modify the program to make it suitable for large deformation or large plasticity analysis by the finite strain approximation method in order to study high stress level creep crack problems.

REFERENCE

1. J.G. Kaufman and Holt, Marshall in Materials Technology, An Inter-American Approach, American Society of Mechanical Engineering, 1968, pp.426-436

2. L.S. Fu, Creep Crack Growth in Technical Alloys at Elevated Temperature ---- A Review, Engng. Fracture Mech. Vol. 13, pp.307-330(1980)

3. G.J. Neate and M.J. Siverns, The Application of Fracture Mechanics to Creep Crack Growth, Int. Conf. On Creep and Fatigue in Elevated Temp. Applications, 234, 1(1974)

4. S. Floreen, The Creep Fracture of Wrought Nickel-Base Alloys by a Fracture Mechanics Approach. Metallurg. Trans. 6A, 1741(1975)

5. L.A. James, Some Preliminary Observations on the Extension of Cracks Under Creep Conditions in Quanched 2 1/4 Cr-Mo Steel, Int. J. Fracture. 9(2), 199-207(1973)

6. J.L. Kenyon, G.A. Webster, J.C. Radon and C.E. Turner, An Investigation of the Application of Fracture Mechanics to Creep Cracking. Int. Conf. on Creep and Fatigue in Elevated Temp. Applications 156, 1(1974)

7. T. Yokobori, T. Kawasaki and M. Horiguchi, Creep Crack Propagation in Austenitic Stainless Steel at Elevated Temp., Proc. 3rd National Congr. on Fracture. Law Tatry Slovakia(1976)

8. C.B. Harrison and G.N. Sander, High-Temp. Crack Growth in Low Cycle Fatigue, Engng. Fracture Mech. 3, 405(1971)

9. R.D. Nickolson and C.L. Formby, the Validity of Various Fracture Mechanics Methods in Creep Temperatures, Int. J. Facture 11, 595(1975)

10. S. Taira, R. Ohtani and A. Nitta, Creep Crack Initiation and Propagation in an 18 Cr - 8 Ni Stainless Steel, Proc. 1973 Symp. on Mechanical Behavior of Materials, 211(1974)

11. S. Taira and R. Ohtani, Creep Crack Propagation and Creep Rupture of Notched Specimens, Int. Conf. on Creep and Fatigue in Elevated Temp. Applications, 213, 1(1974)

12. S. Taira and R. Ohtani, Crack Propagation in Creep, Proc. of 2nd Int. Conf. on Mech. Behav. of Mat., Boston, (1976), pp.465-509, Special Volume, American Society of Metals, (1978) pp.155-182

13. P.L. Jones and A.S. Tetelman, Characterization of the Elevated Temperature Static Load Crack Extension Behavior of Type 304 Stainless Steel, Engng. Fracture Mech. 12, 79-97(1979)

14. B.L. Freeman, The Estimation of Creep Crack Growth by Reference Stress Method, Int. J. Facture 15(2), 179-190(1979)

15. J.R. Haigh, The Growth of Fatigue Cracks at High Temperature Under Predominately Elastic Loading, Engng. Facture Mech., 271-284(1975)

16. V. Vitek, A Theory of the Initiation of Creep Crack Growth, Int. J. Fracture 13, 39-50(1977)

17. R. Pilkington, D. Hutchinson and C.L. Jones, High-Temperature Crack Opening Displacement Measurements in a Ferrite Steel, Metallurgical Sci. J. 8, 237-241(1974)

18. J.D. Landes and J.A. Begley, A Fracture Mechanics Approach to Creep Crack Growth, Report 74-1E7-FESGT-P1, Westinghouse Research Laboratory, December 1974

19. G.A. Webster, The Application of Fracture Mechanics to Creep Cracking, Conference on Mechanics and Physics of Fracture, Institute of Physics, Cambridge, Paper 18, 1975

20. K.M. Nikbin, G.A. Webster and C.E. Turner, A Comparison of Methods of Correlating Creep Crack Growth, in Fracture 1977, 2, ICF4, Waterloo, Canada, 19-24 June 1977

21. M.P. Harper and E.G. Ellison, The Use of the C* Parameter in Predicting Creep Crack Propagation Rates, J. Strain Analysis, 12, 167-179(1977)

22. H. Riedel and J.R. Rice, Tensile Cracks in Creeping Solids, Fracture Mechanics: Twelfth Conference, ASTM STP 700, 1980, pp. 112-130

23. R. Koterazawa and T. Mori, Applicability of Fracture Mechanics Parameters to Crack Propagation under Creep Conditions, Trans. of the ASME 298-305, Vol.99, Oct. 1977

24. A. Saxena, Evaluation of C^* for the Characterization of Creep-Crack-Growth Behavior in 304 Stainless Steel, Fracture Mechanics: Twelth Conference, ASTM STP 700, 1980, pp. 131-151

25. V.M. Radhakrishnan and A.J. McEvily, A Critical Analysis of Crack Growth in Creep, Trans. of the ASME 200-206, Vol. 102, April 1980

26. S.N. Atluri, Path-Independent Integrals in Finite Elasticity and Inelasticity, with Body Forces, Inertia and Arbitrary Crack-Face Conditions Rep. GIT-CACM-SNA-81-8, Georgia Institute of Technology, March, 1981, also Engng. Fracture Mech.(in press)

27. R.B. Stonesifer and S.N. Atluri, On a Study of the $(\Delta T)_c$ and C^* Integrals for Fracture Analysis under Non-Steady Creep, Engng Fracture Mech. Vol. 16, No. 5, pp.625-643, 1982

28. R.B. Stonesifer and S.N. Atluri, Moving Singularity Creep Crack Growth Analysis with the $(\Delta T)_c$ and C^* Integrals, Engng Fracture Mech. Vol.16, No.6, pp.769-782, 1982

29. Y.J. Liu and T.R. Hsu, A General Treatment of Creep Crack Growth, to be published.

30. N.L. Goldman and J.W. Hutchinson, Fully Plastic Crack Problems: The Center Crack Strip under Plane Strain, Harvard University, Cambridge, Mass., (1973)

31. H. Riedel, Creep Deformation at Crack Tips in Elastic-Viscoplastic Solids, J. Mech. Phys. Solids, Vol 29, pp.35-49(1981)

32. C.Y. Hui and H. Riedel, The Asymptotic Stress and Strain Field Near the Tip of a Growing Crack under Creep Conditions, Int. Journ. of Fracture, 17(1981), pp.409-425

33. L.N. McCartney, On the Energy Balance Approach to Fracture in Creeping Materials, Int. Journ. of Fracture, 19(1982), pp.99-113

34. S. Kubo, K. Ohji and K. Ogura, An Analysis of Creep Crack Propagation on the Basis of the Plastic Singular Stress Field, Engng. Fracture Mech., Vol.11, pp.315-329(1979)

35. L.N. McCartney, Derivation of Crack Growth Laws for Linear Visco-Elastic Solids Based upon the Concept of a Fracture Process Zone, Int. J. Fracture Vol.16, No.4(1980)

36. J.T. Barnby, Crack Propagation during Steady State Creep, Engng. Fracture Mech. 7, pp.299-304(1975)

37. K.C. To, A Phenomenological Theory of Subcritical Creep Crack Growth under Constant Loading in an Inert Environment, Int. J. Fracture 11, 641(1975)

38. S. Purushothaman and J.K. Tien, A Theory for Creep Crack Growth, Scripta Metallurgica 10, 663-666(1976)

39. V. Vitek, A Theory of the Initiation of Creep Crack Growth, Int. J. Fracture 13, 39-50(1977)

40. R. Ohtani, Finite Element Analysis and Experimental Investigation on Creep Crack Propagation, Creep in Structures, ed. A.R.S. Ponter and D.R. Hayhurst, IUTAM, (1980)

41. H.P. Van Leeuwen, The Application of Fracture Mechanics to Creep Crack Growth, Engng. Fracture Mech., Vol.9, pp.951-974(1977)

42. H. Riedel, The Extension of a Macroscopic Crack at Elevated Temperature by the Growth and Coalescence of Microvoids, Creep in Structures, Edited by A.R.S. Ponter and D.R. Hayhurst, P.504, Springer-Verlag, (1981)

43. T.R. Hsu, A.W.M. Bertels, S. Banerjee and W.C. Harrison, Theoretical Basis for a Transient Thermal Elasto-Plastic Stress Analysis of Nuclear Reactor Fuel Element, Whiteshell Nuclear Research Establishment Report AECL-5233, Atomic Energy of Canada(1976)

44. Y. Yamada, N. Yoshimura and T. Sakurai, Plastic Stress-Strain Matrix and its Application for the Solution of Elastic-Plastic Problems by the Finite Element Method, International Journal of Mechanical Science 10, pp.343-354, (1968)

45. R.K. Penny and A.W.M. Bertels, Propagation and Opening of a Through Crack in a Pipe Subject to Combined Cyclic Thermo-Mechanical Loadings, J. of Pressure Vessel Technology, ASME Trans., Feb, 1976. pp. 17-25

46. I.C. Cormeau, Numerical Stability in Quasi-Static Elasto-Viscoplasticity, Int. J. Num. Meth. Engng. 9, 109-127(1975)

47. B. Irons and G. Treharne, A Bound Theorem in Eigenvalues and its Practical Applications, Proc. 3rd Conf. Matrix Meth. Struct. Mech. pp. 245-254, Wright-Patterson A.F.B., Ohio(1973)

48. D. Broek, Elementary Engineering Fracture Mechanics, Noordhoff International Publishing, LEYDEN

49. I.s. Tuba, A Method of Elastic-Plastic Plane Stress and Strain Analysis, J. Strain Analysis 1, pp.115-122, (1966)

50. J.R. Rice and G.F. Rosengren, Plane Strain Deformation Near a Crack Tip in a Power-Law Hardening Material, J. Mech. phys. Sol., 16, pp.1, (1968)

51. D. Broek, A Study on Ductile Fracture, Nat. Aerospace Inst. Amsterdam, Rept. TR 71021(1971)

52. G.R. Irwin, Plastic Zone Near a Crack and Toughness, Proc. 7th Sagamore Conf. P.IV-63(1960)

53. D.S. Dugdale, Yielding of Steel Sheets Containing Slits, J. Mech. Phys. Sol., 8(1960) pp. 100-108

54. F.M. Burdekin and D.E.W. Stone, The Crack Opening Displacement Approach to Fracture Mechanics in Yielding Materials, J. Strain Analysis, 1(1966) pp.145-153

55. J.M. Kraft, A.M. Sullivan and R.W. Boyle, Effect of Dimensions on Fast Fracure Instability of Notched Sheets, Proc. of the Crack-Propagation Symposium I, pp.8-28, Cranfield(1961)

56. J.R. Rice, Mathematical Analysis in the Mechanics of Fracture, Fracture: An Advanced Treatise, Edited by Liebowitz, H., Acadamic Press, New York, Vol.2 (1968), pp.191-311

57. J.R. Rice, A Path Independent Integral and the Approximate Analysis of Strain Concentrations by Notches and Cracks, J. Appl. Mech. (1968) pp.379-386

58. J.D. Landes and J.A. Begley, The Effect of Specimen Geometry on J_{IC} , ASTM STP 514 (1972), pp.24-39

59. J.A. Begley and J.D. Landes, The J - Integral as a Fracture Criterion, ASTM STP 514(1972), pp.1-20

60. A.A. Wells, Unstable Crack Propagation in Metals-Cleavage and Fast Fractuer, Proc. Crack Propagation Symposium, Granfield(1961), pp.210-230

61. A.A. Wells, Application of Fracture Mechanics at and Beyond General Yielding, British Welding Research Ass. Rep. M13, (1963)

62. B.J. Scheaeffer, H.W. Liu and J.S. Ke, Deformation and the Strip Necking Zone in a Cracked Steel Sheet, Experimental Mechanics 11(1971), pp.172-175

63. W.J. Gavigan, J.S. Ke and H.W. Liu, Local and Gross Deformations in Cracked Metallic Plates, Int. Jour. of Frac. 9(1973), pp.255-266

64. W.T. Evans, M.F. Light and A.R. Luxmoore, An Experimental and Finite Element Investigation of Fracture in Aluminum Thin Plates, J. Mech. Phys. Sol. 28(1980), pp.167-189

65. G.E. Dieter, Mechanical Metallurgy, McGraw-Hill, New York (1976)

66. W.S. Dorn and D.D.M Cracken, Numerical Methods with Fortran IV Case Study, John Wiley & Sons, New York, (1972)

67. H. Anderson, A Finite-Element Representation of Stable Crack-Growth, Jour. of Mech. and Phy. Sol. 21(1973), pp.337-356

68. J.R. Rice and E.P. Sorensen, Continuing Crack-Tip Deformation and Fracture for Plane-Strain Crack Growth in Elastic-Plastic Solids, Jour. mech. phy. sol. 26(1978), pp.163-186

69. Y.J. Kim, Stable Crack Growth in Ductile Materials ------ A Finite Element Approach, Ph.D Thesis, Dept. Mech. Engng. U. of Manitoba, Canada

70. Y.J. Kim and T.R. Hsu, A Numerical Analysis on Stable Crack Growth under Increasing Load, Int. Jour. of Frac., Vol.00, No.0, pp.1-15, (1981)

71. K. Ohji et al, Trans. JSME, 44, (1978) pp. 1831

72. T.R. Hsu, Y.J. Liu and Z.H. Zhai, On the Numerical Evaluation of C* - Integral for Creep Fracture Analysis, Accepted by the International Symposium on Fracture Mechanics, Beijing, China, 1983

73. C.F. Shih, H.G. Delorenzi and W.R. Andrews, Studies on Crack Initiation and Stable Crack Growth Elastic-Plastic Fracture, ASTM STP 668, pp.65-121

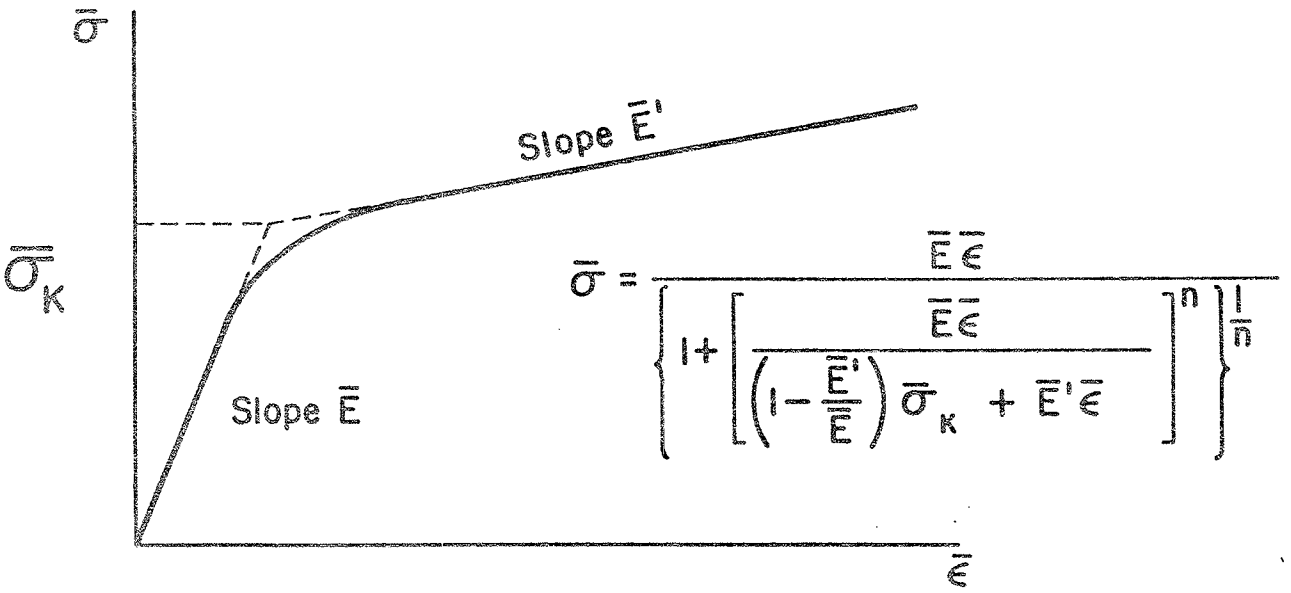

Fig. 1 Power law approximation of a typical stress strain relation

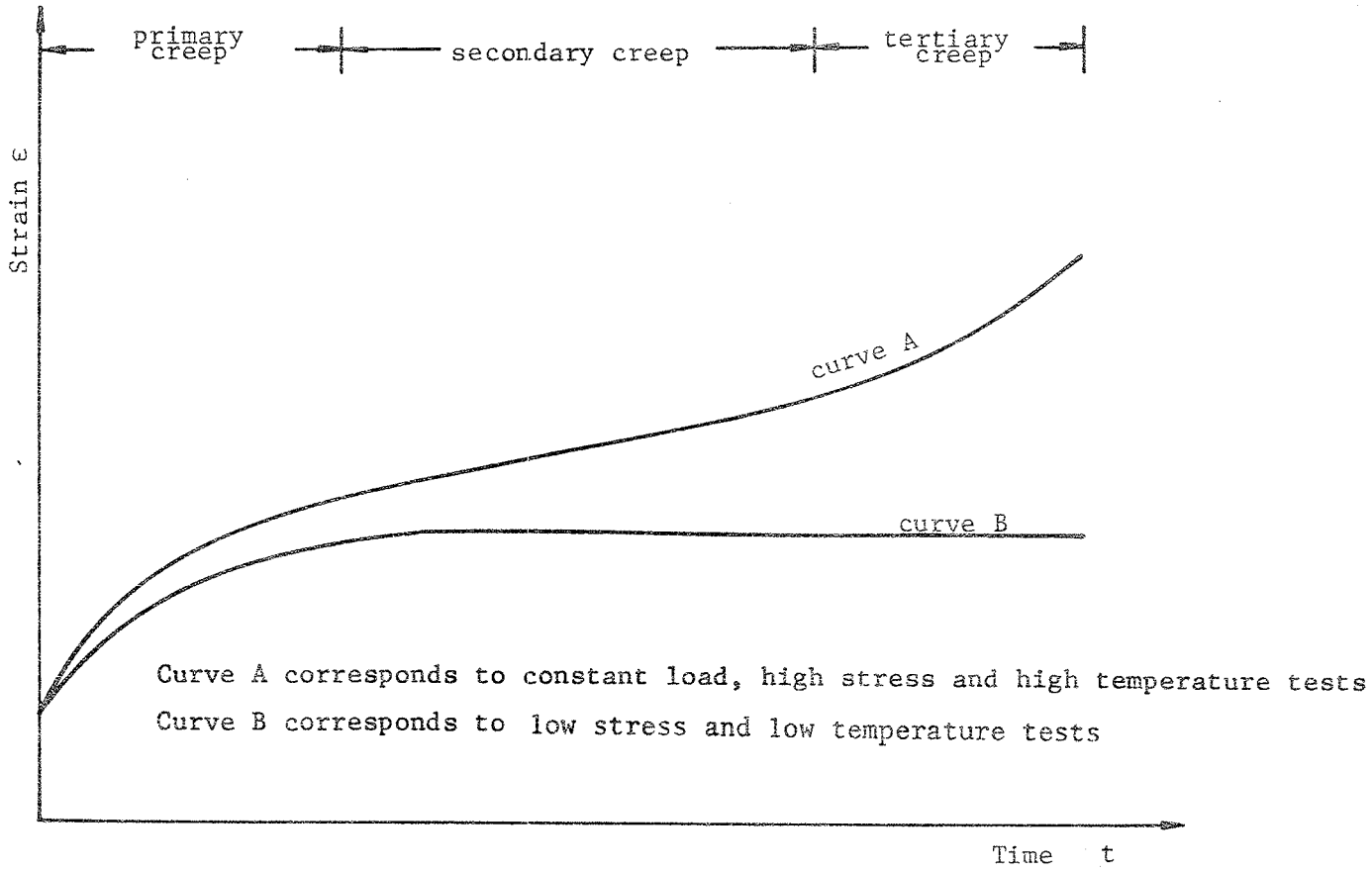

Fig. 2 Typical strain variations of materials during creep deformation

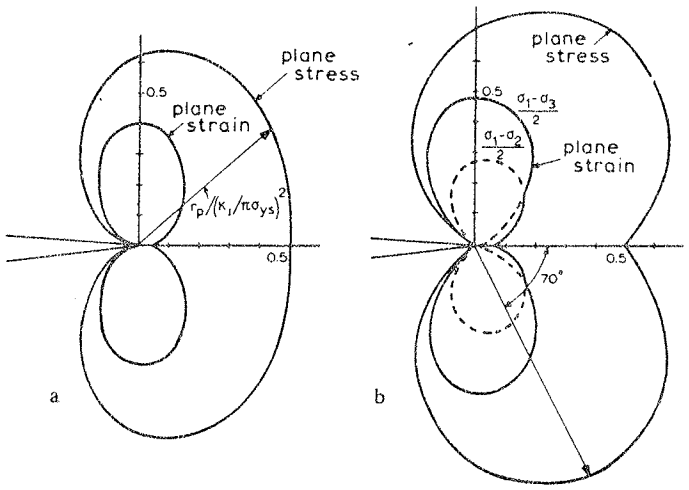

Fig. 3 Plastic zone shapes according to
a. Von Mises criterion
b. Tresca criterion

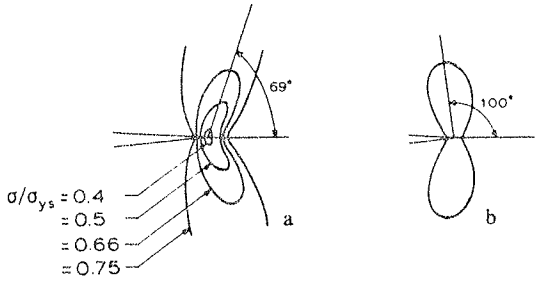

Fig. 4 More accurate plastic zone shapes according to
a. Tuba b. Rice and Rosengren

A. Photograph of a cracked specimen showing a high shear region
(Zero stress at left, onset of crack growth at right.) [51]

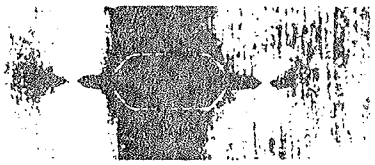

B. Creep crack growth in 304 s.s. specimen [40]

Fig.5 Photographs showing plastic zone

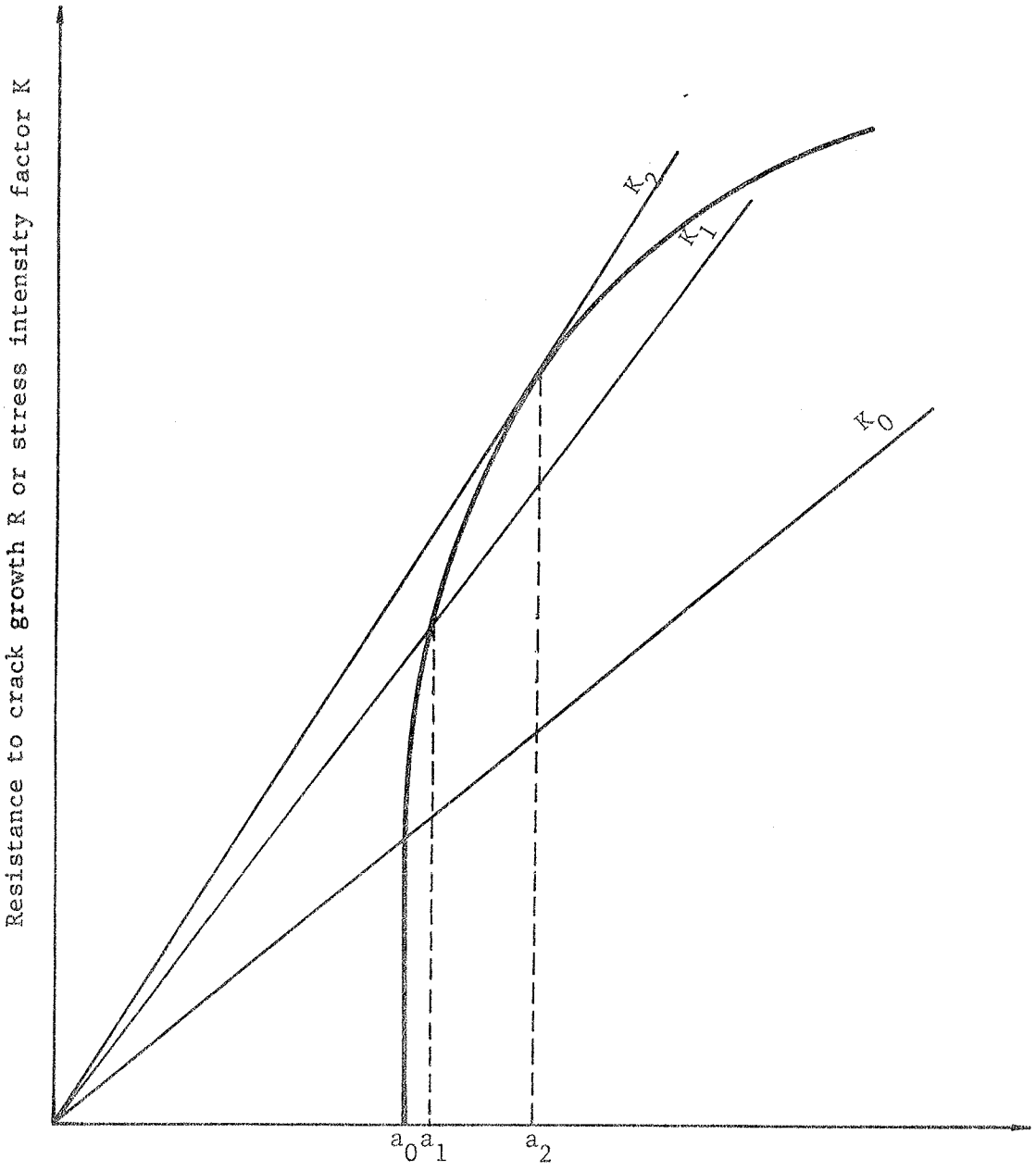

Fig. 6 A typical R-curve for ductile materials

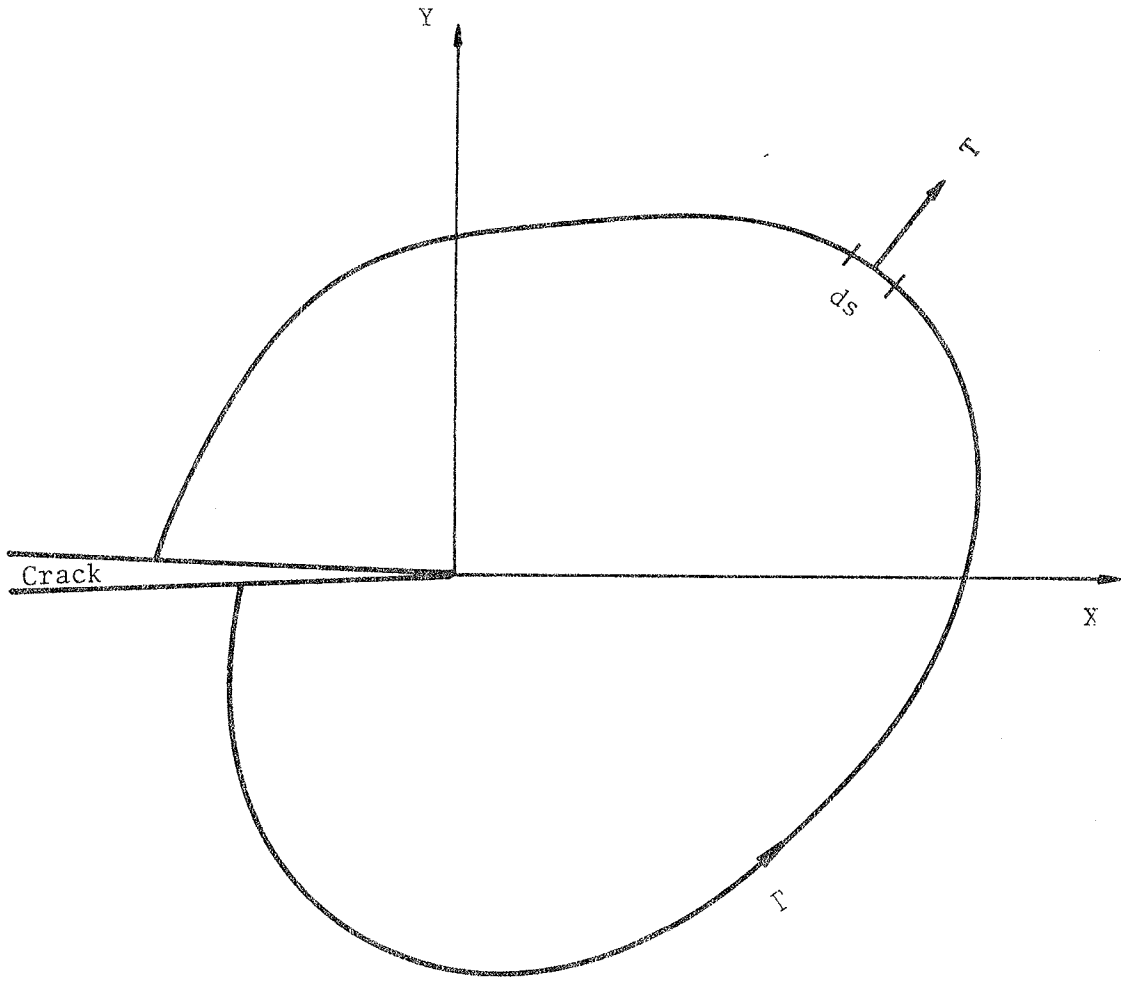

Fig. 7 The contour for the J - integral

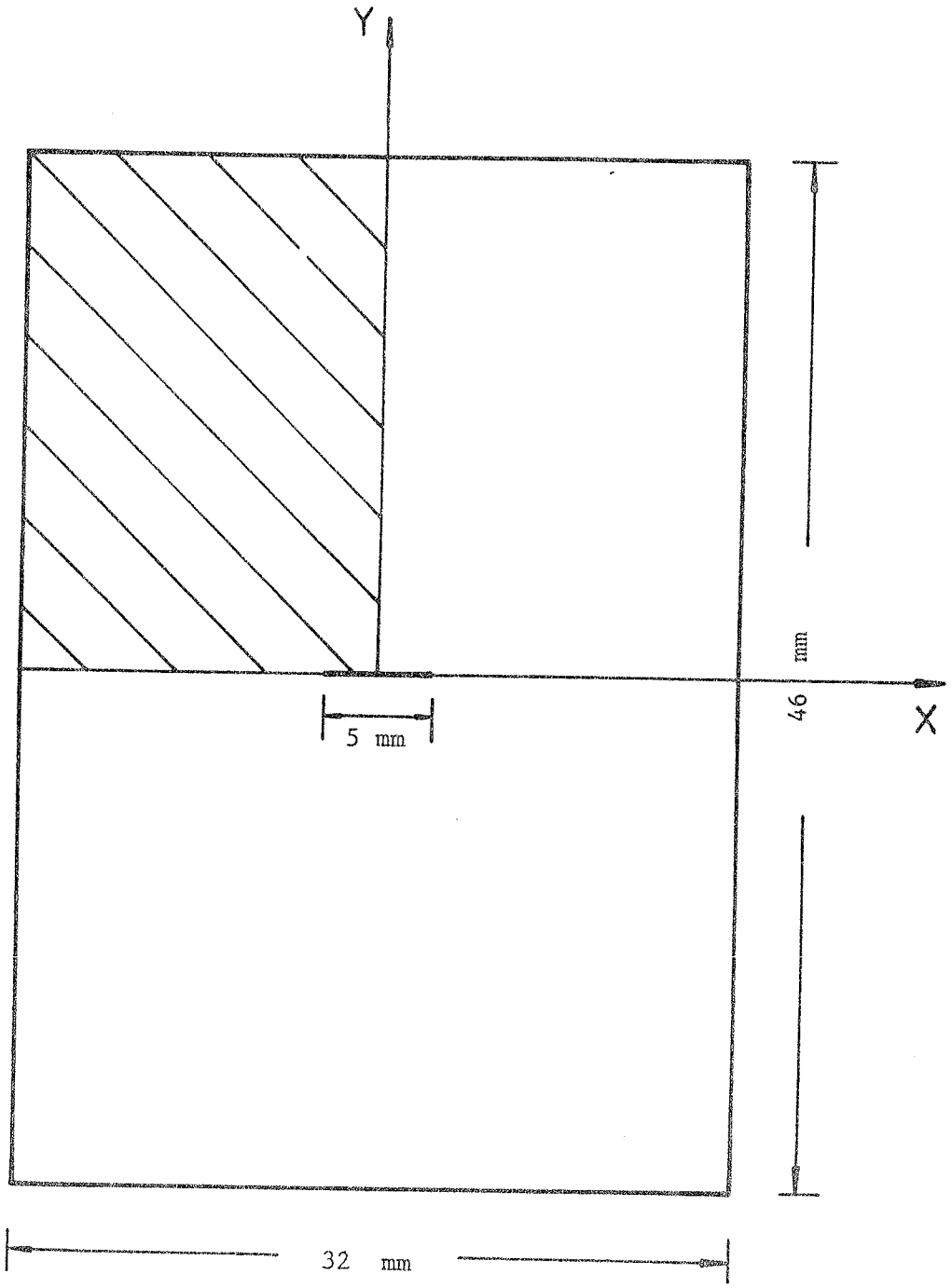

Plate thickness = 2.3 mm

Fig. 8 A centre cracked plate

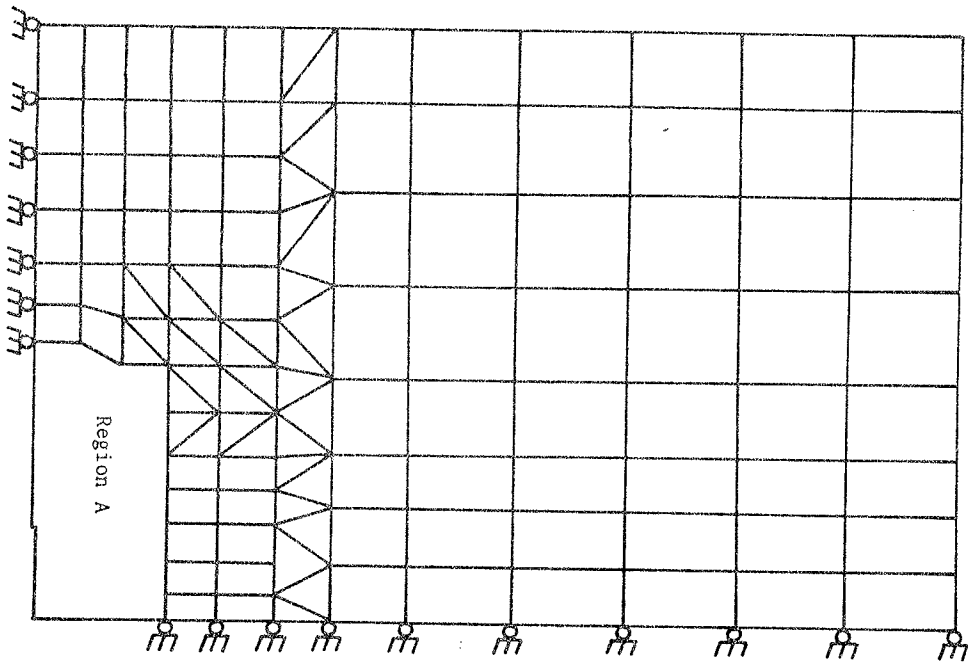

A. Overall mesh

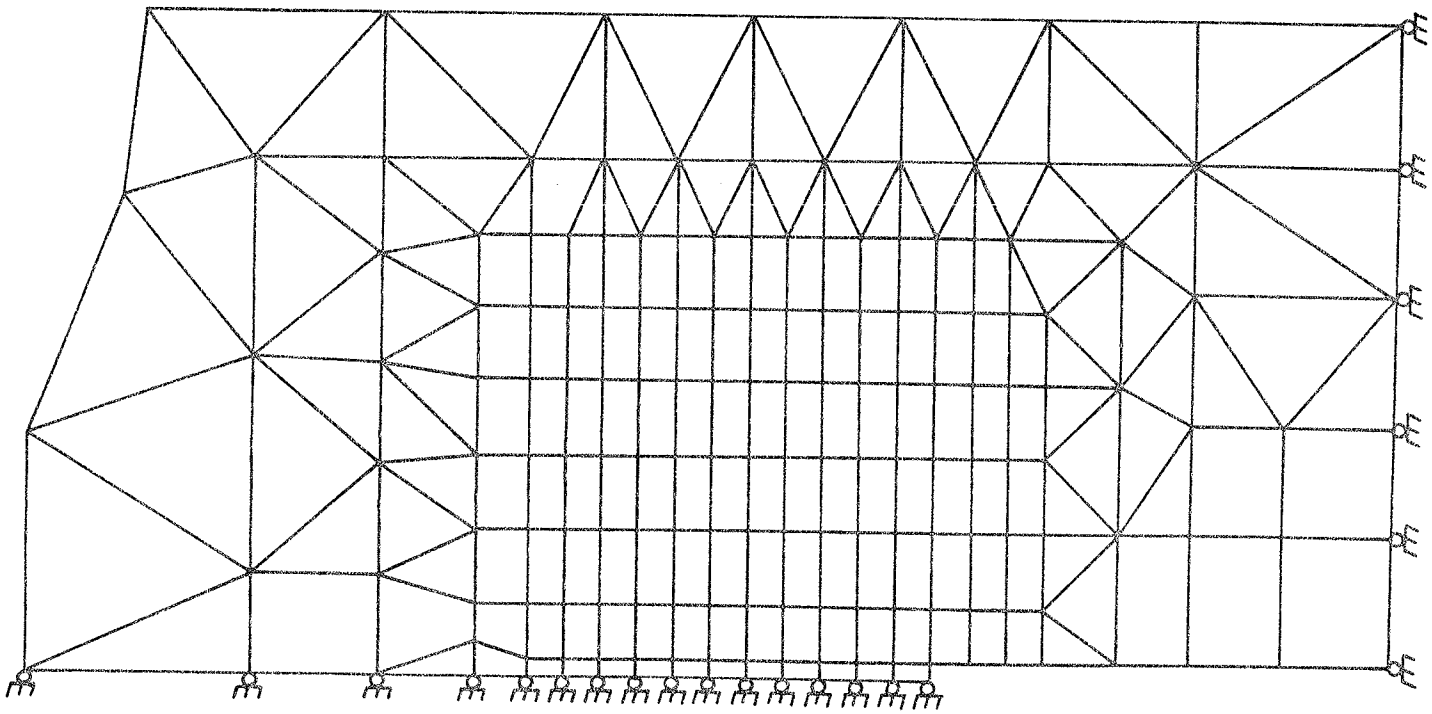

B. Detail of region A

Fig. 9 Finite element mesh

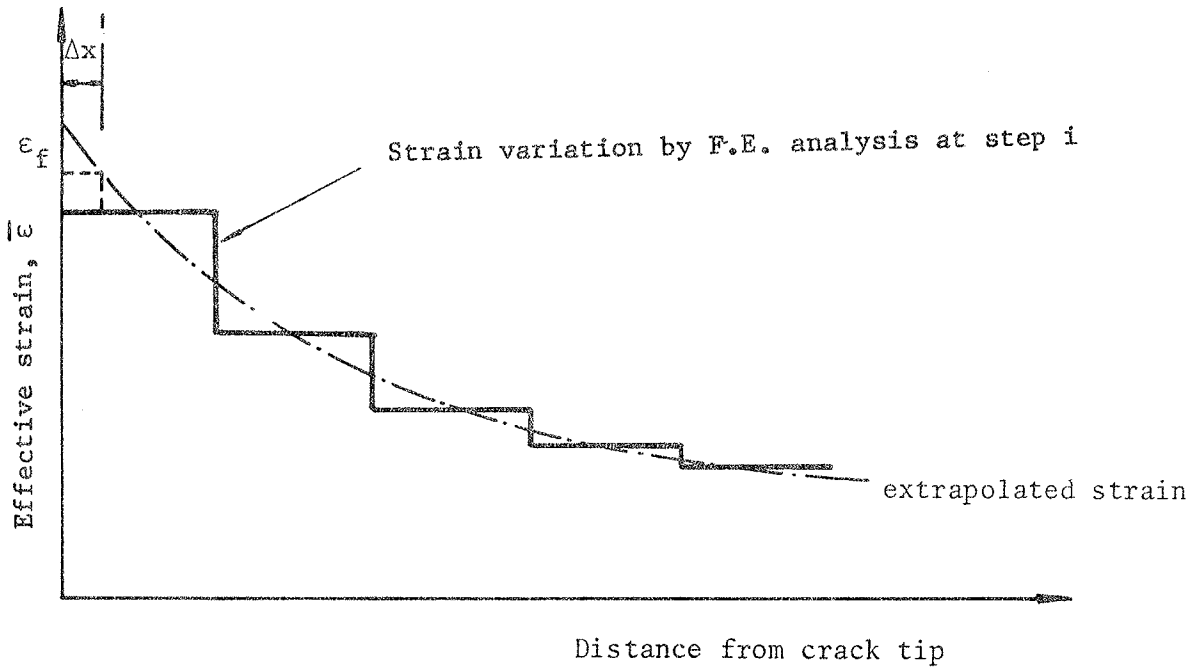

Fig. 10 Crack extension at time step i

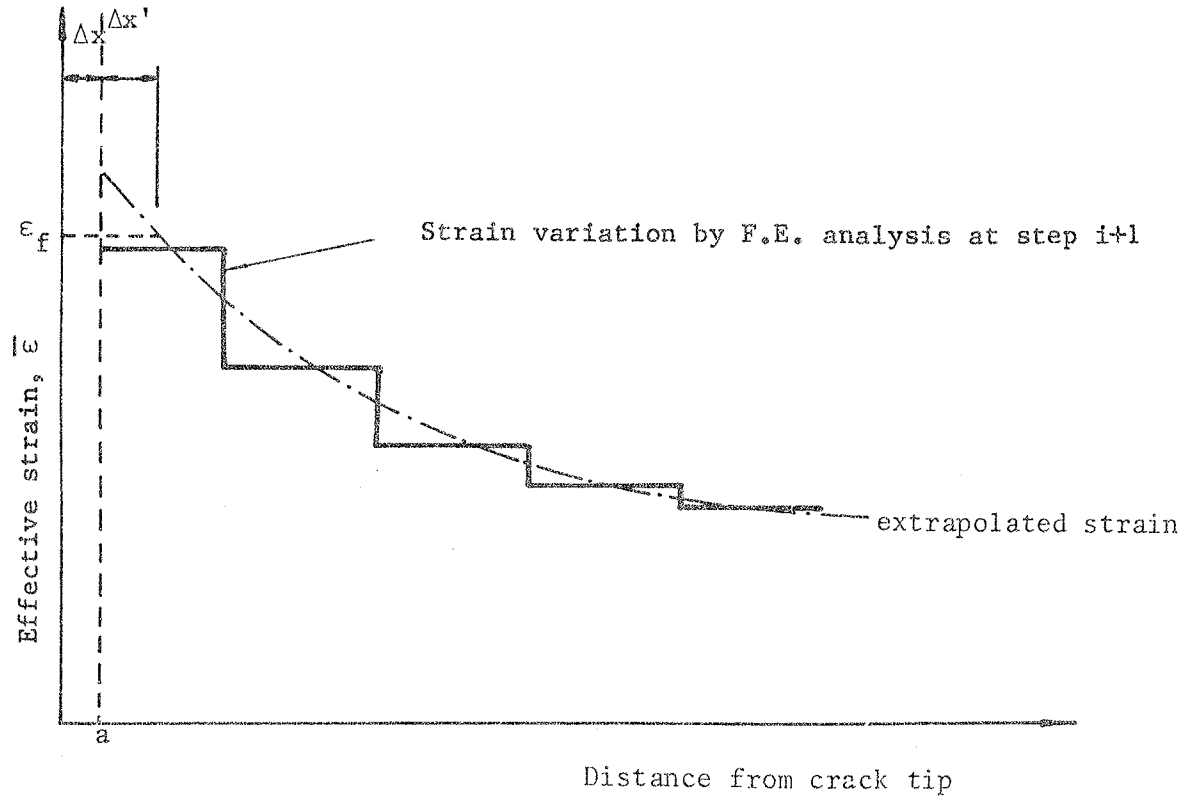

Fig. 11 Crack extension at time step i+1

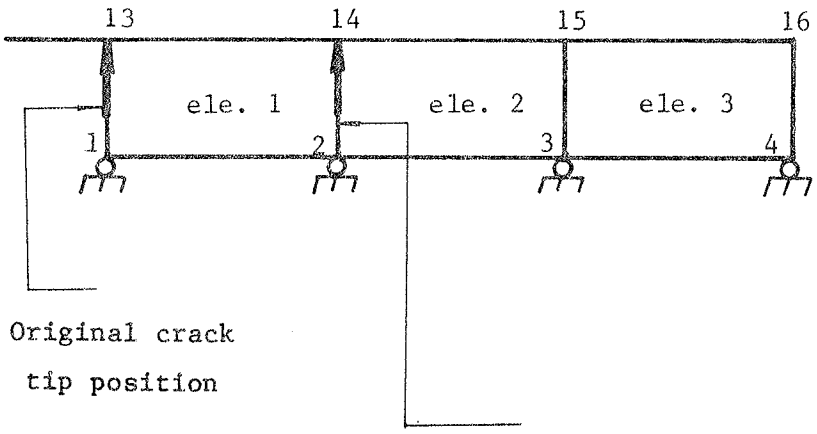

Fig. 12 Nodal force relaxation

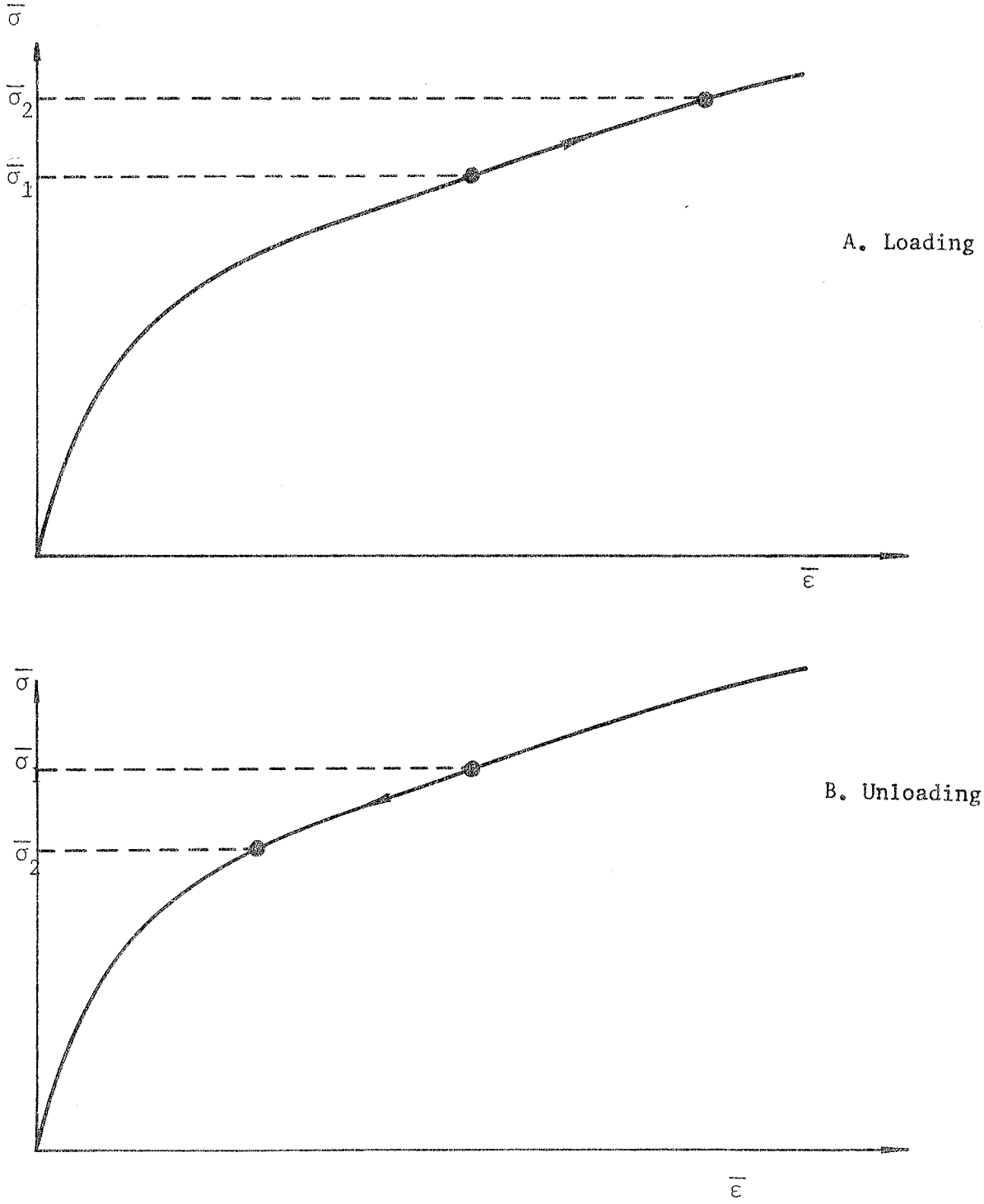

Fig. 13 Loading and unloading

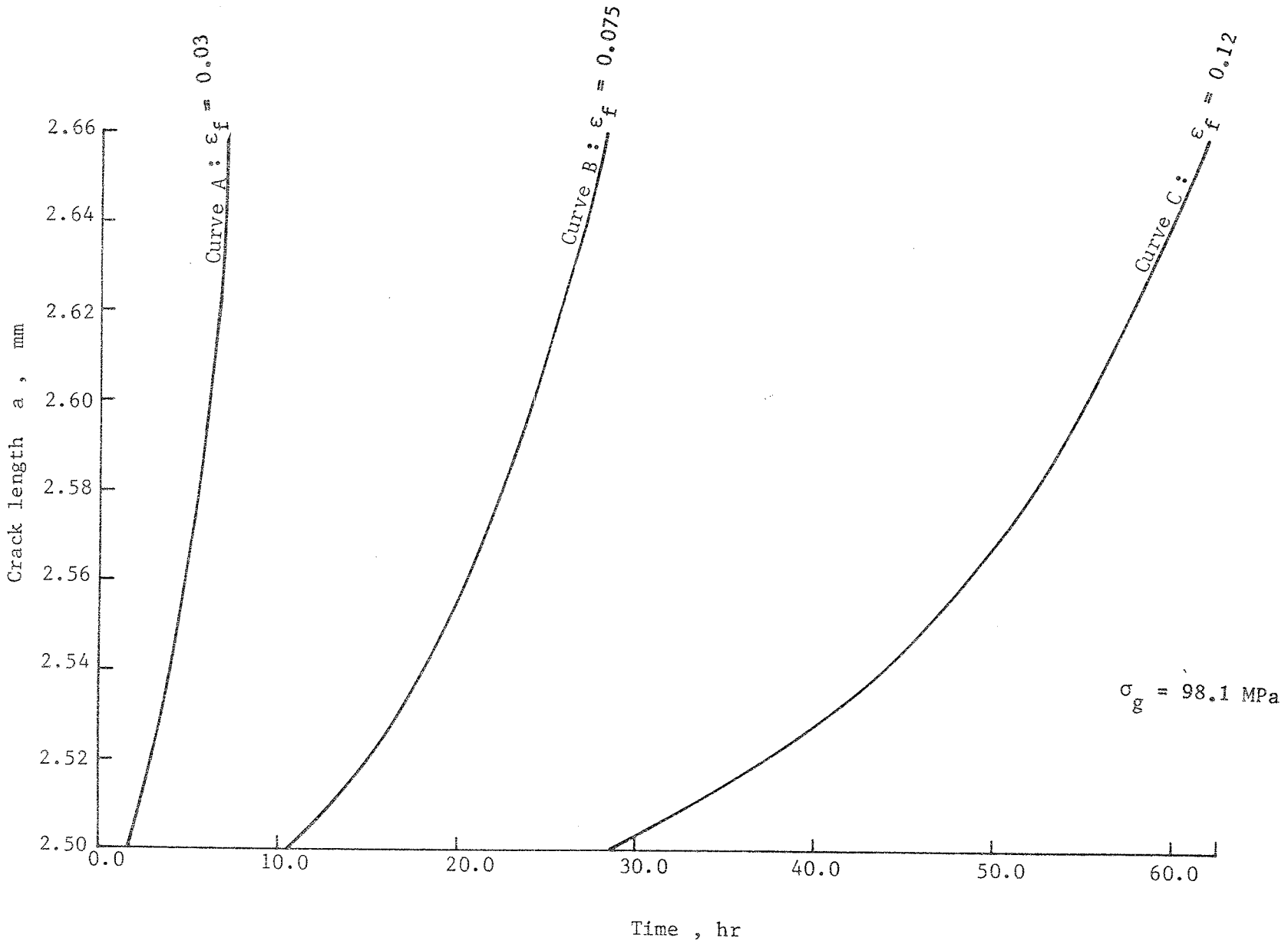

Fig. 14 The relationship between crack length and time

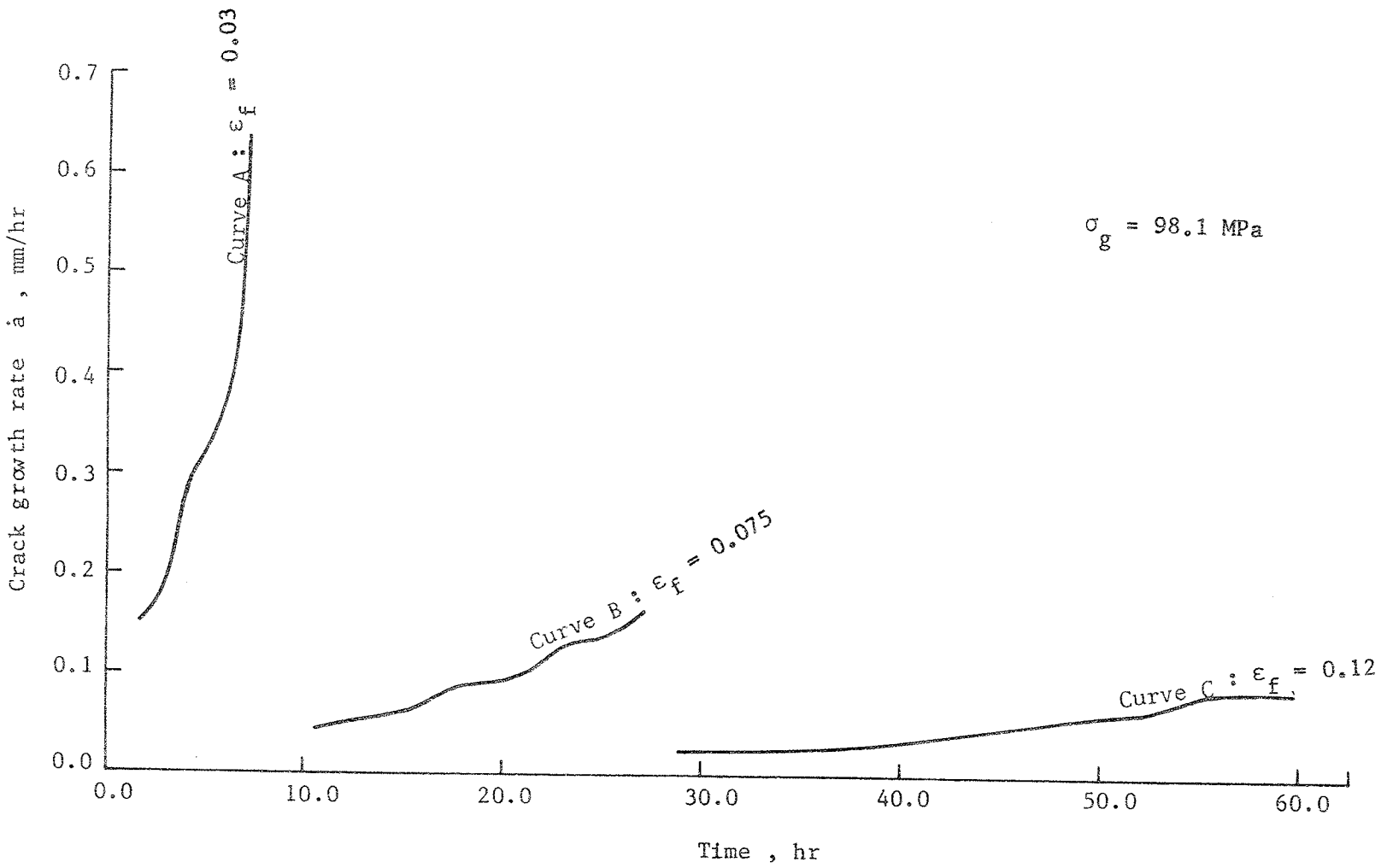

Fig. 15 The relationship between crack growth rate and time

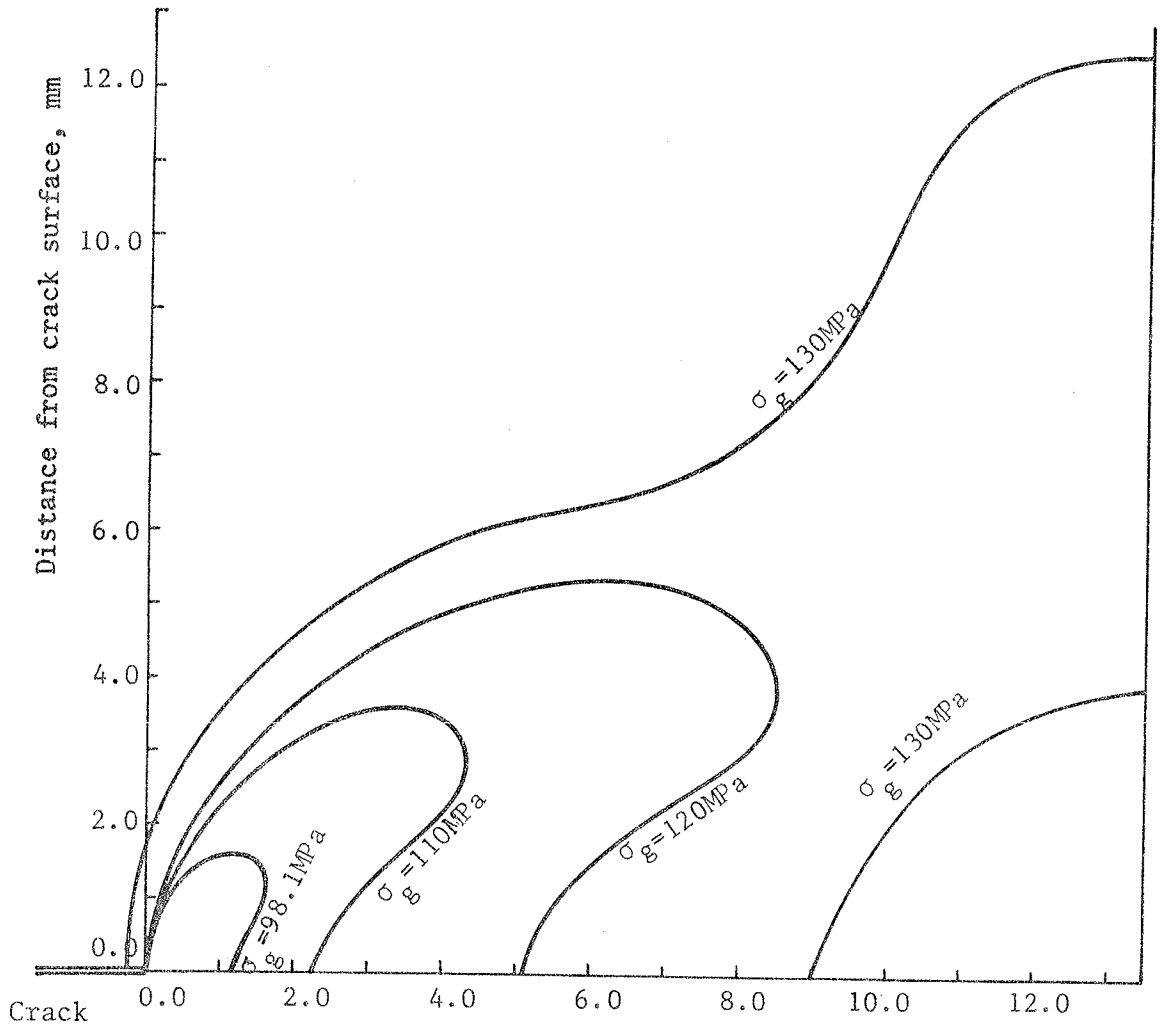

Fig. 16 Shape of plastic zone under various gross stresses

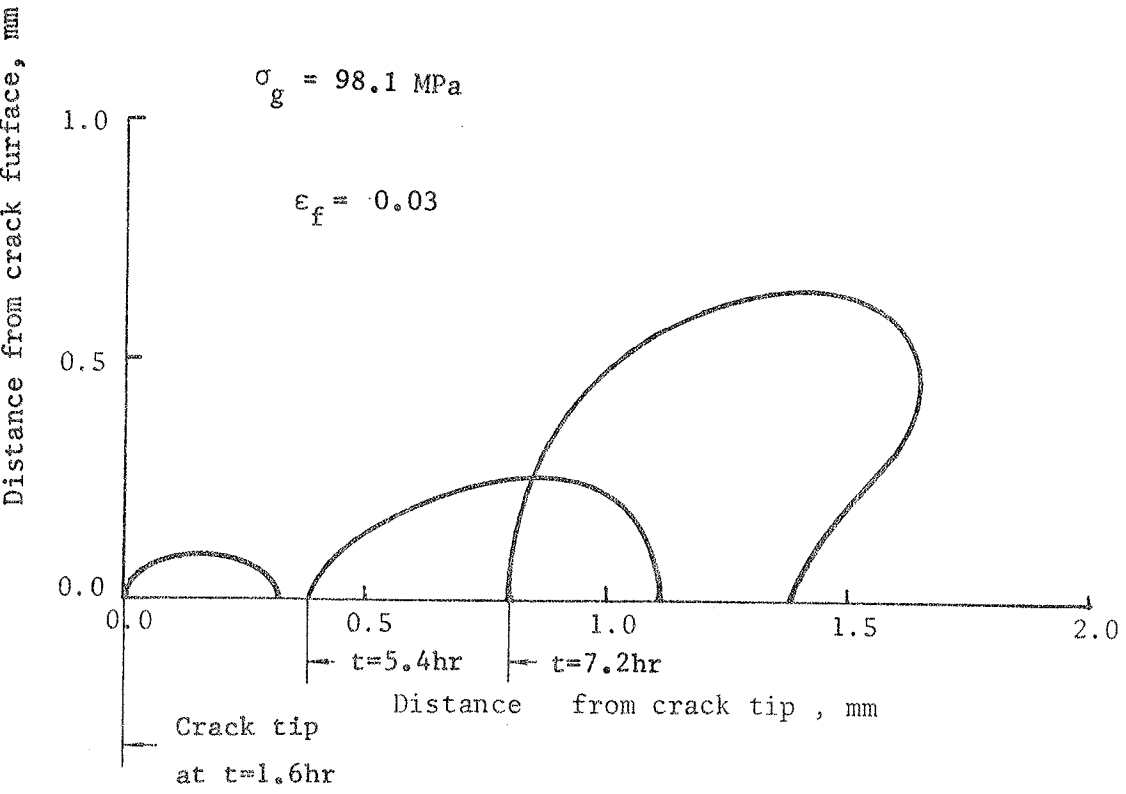

Fig. 17 Variation of plastic zone in the process of crack propagation

σ_g = 98.1 MPa

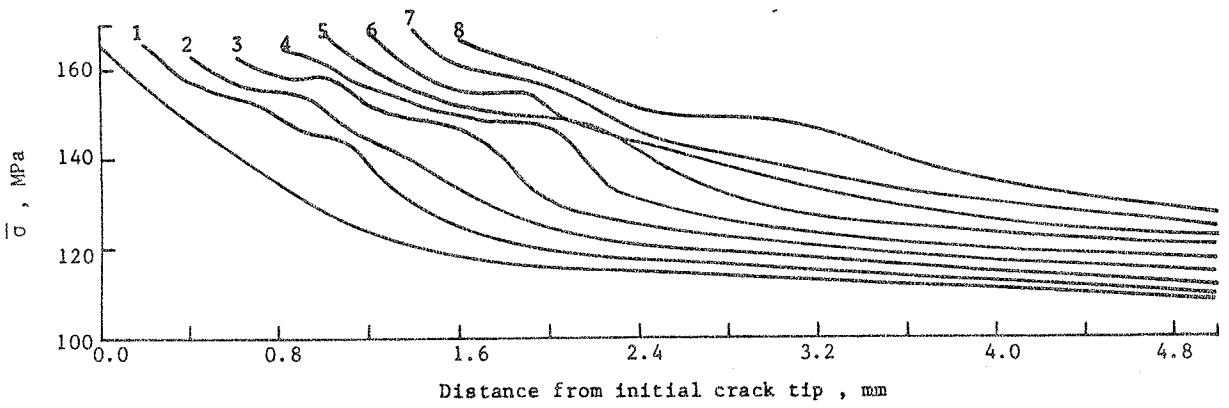

A. ε_f = 0.03

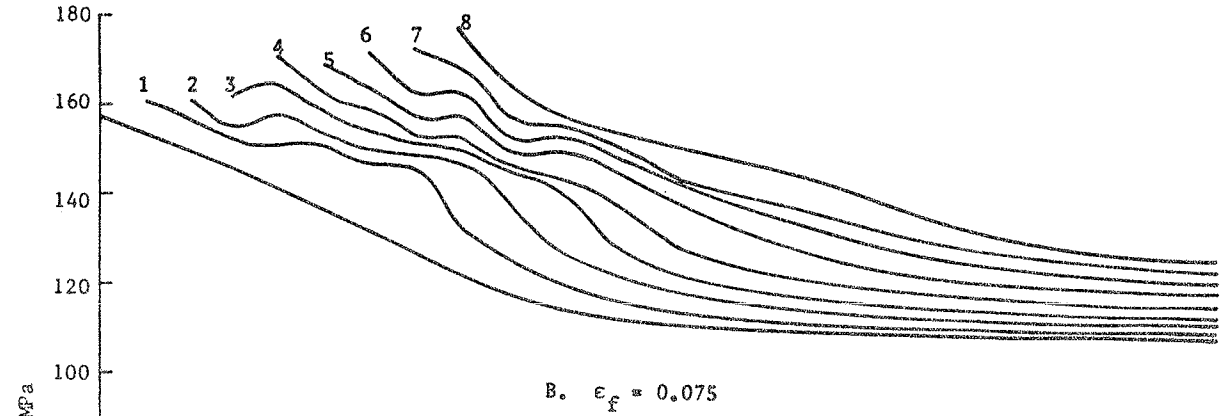

B. ε_f = 0.075

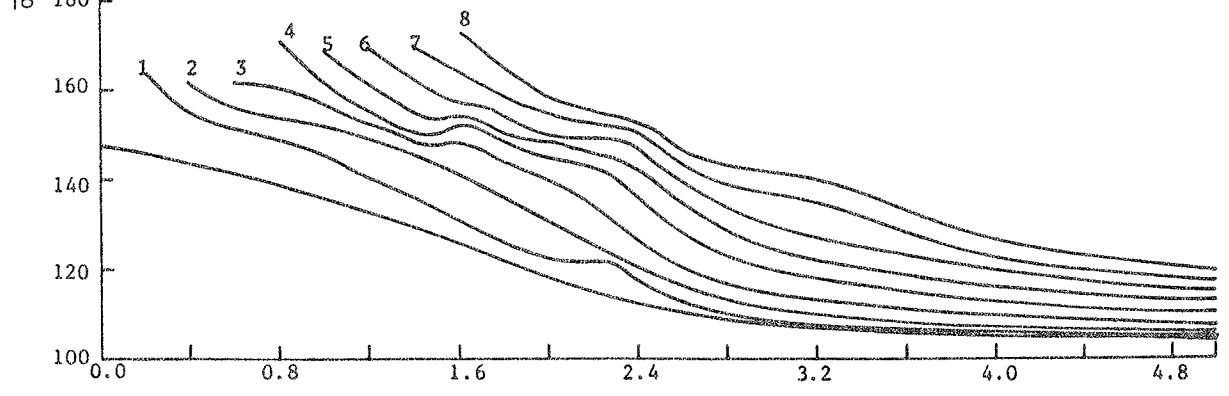

C. ε_f = 0.12

Fig.18 Effective stress distribution ahead of crack tip

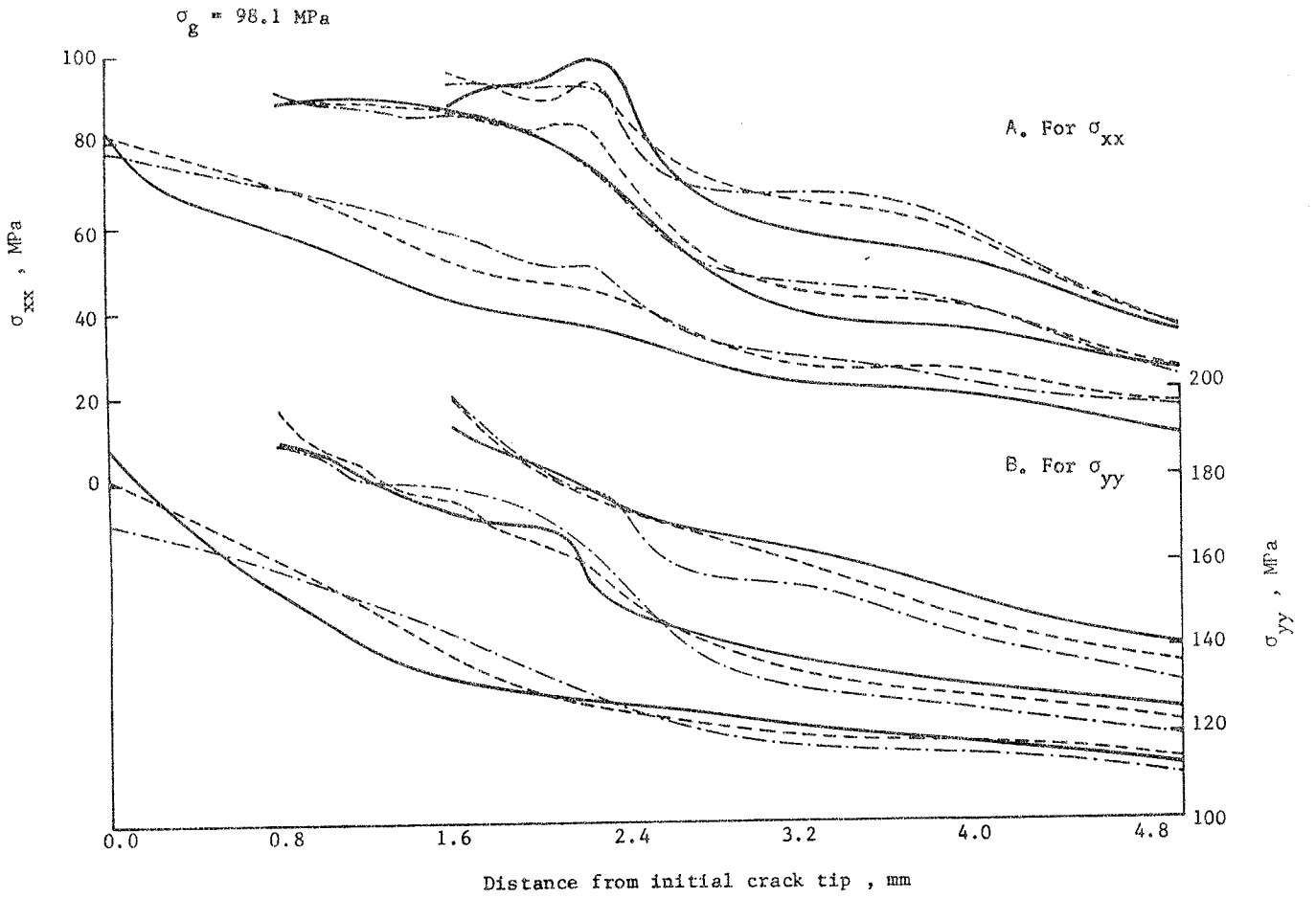

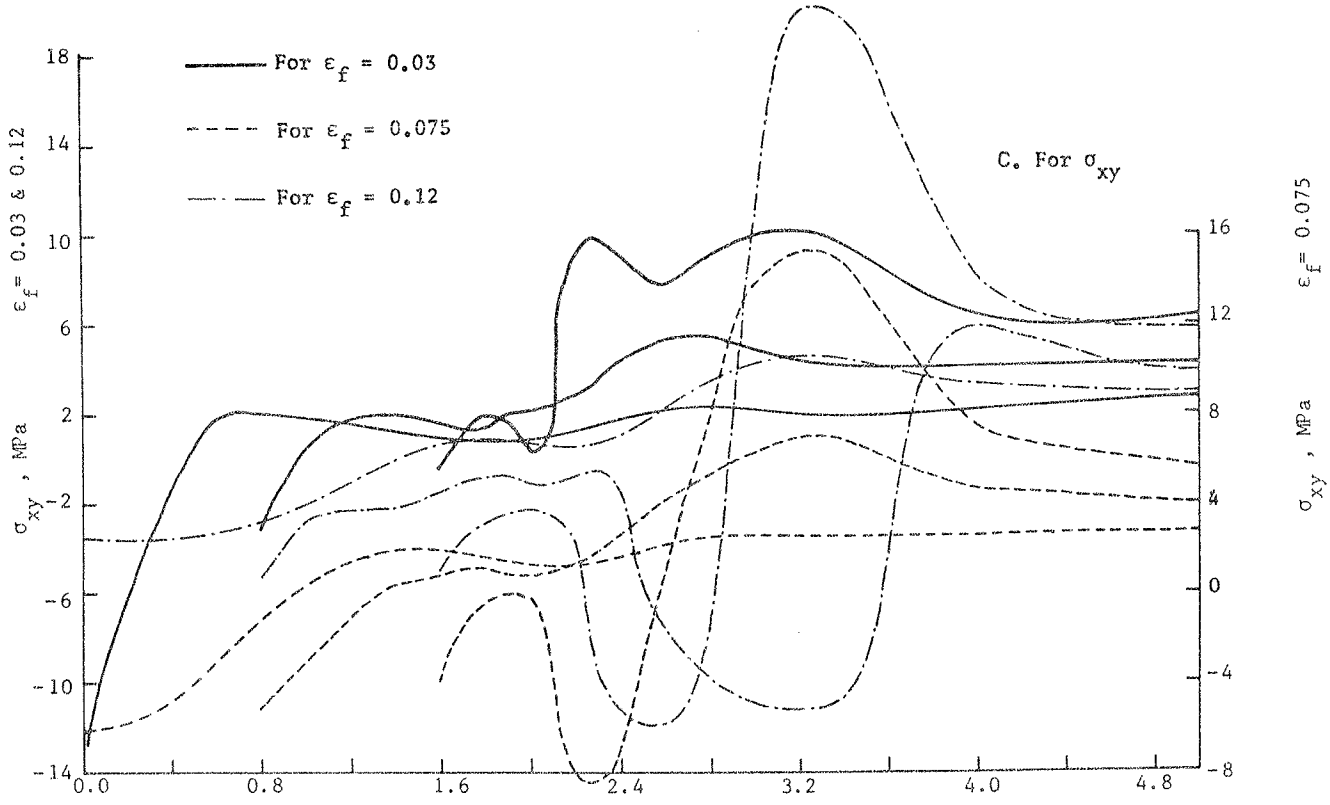

Fig. 20 Stress components ahead of crack tip

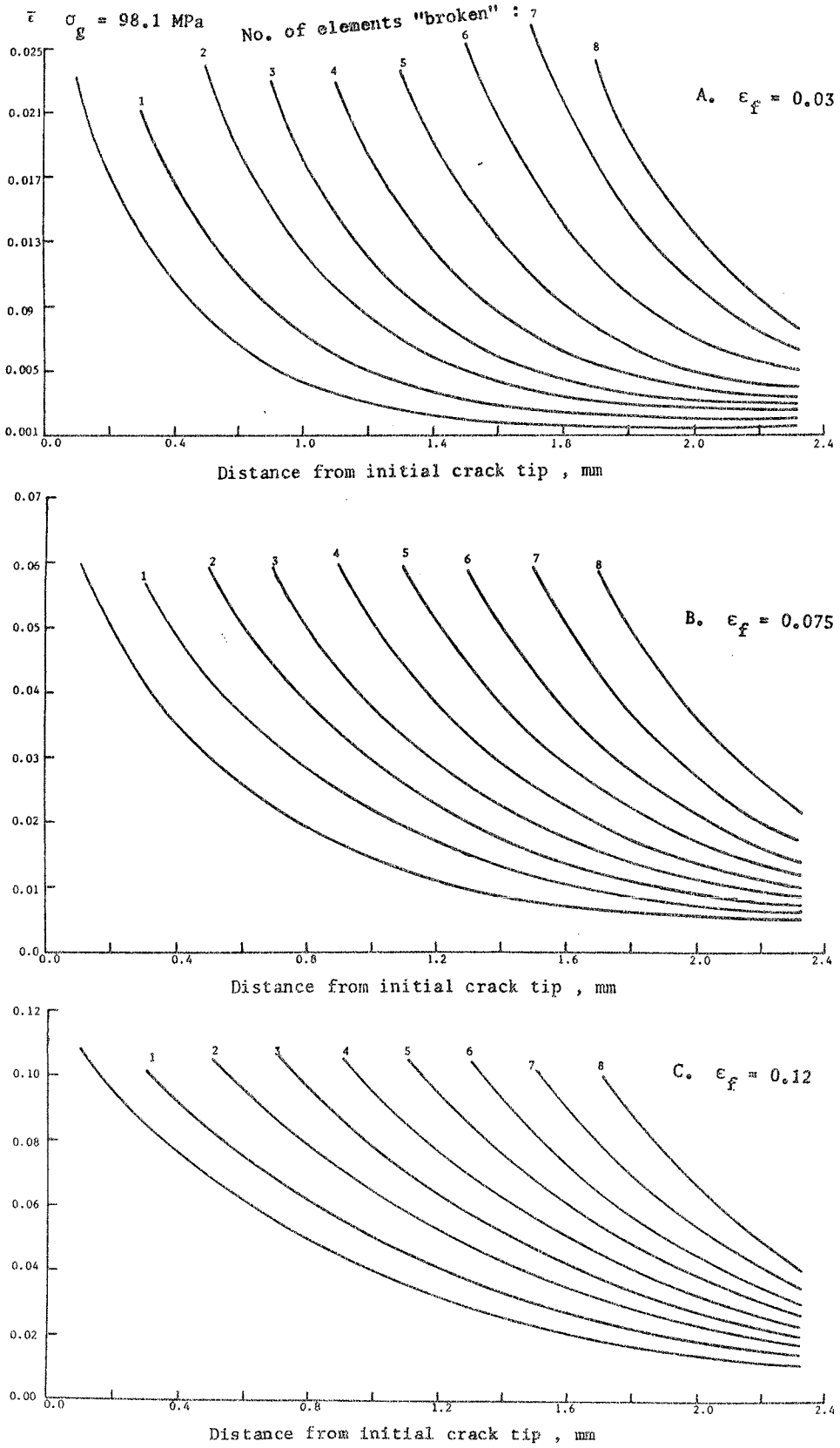

Fig.21 Effective strain distribution

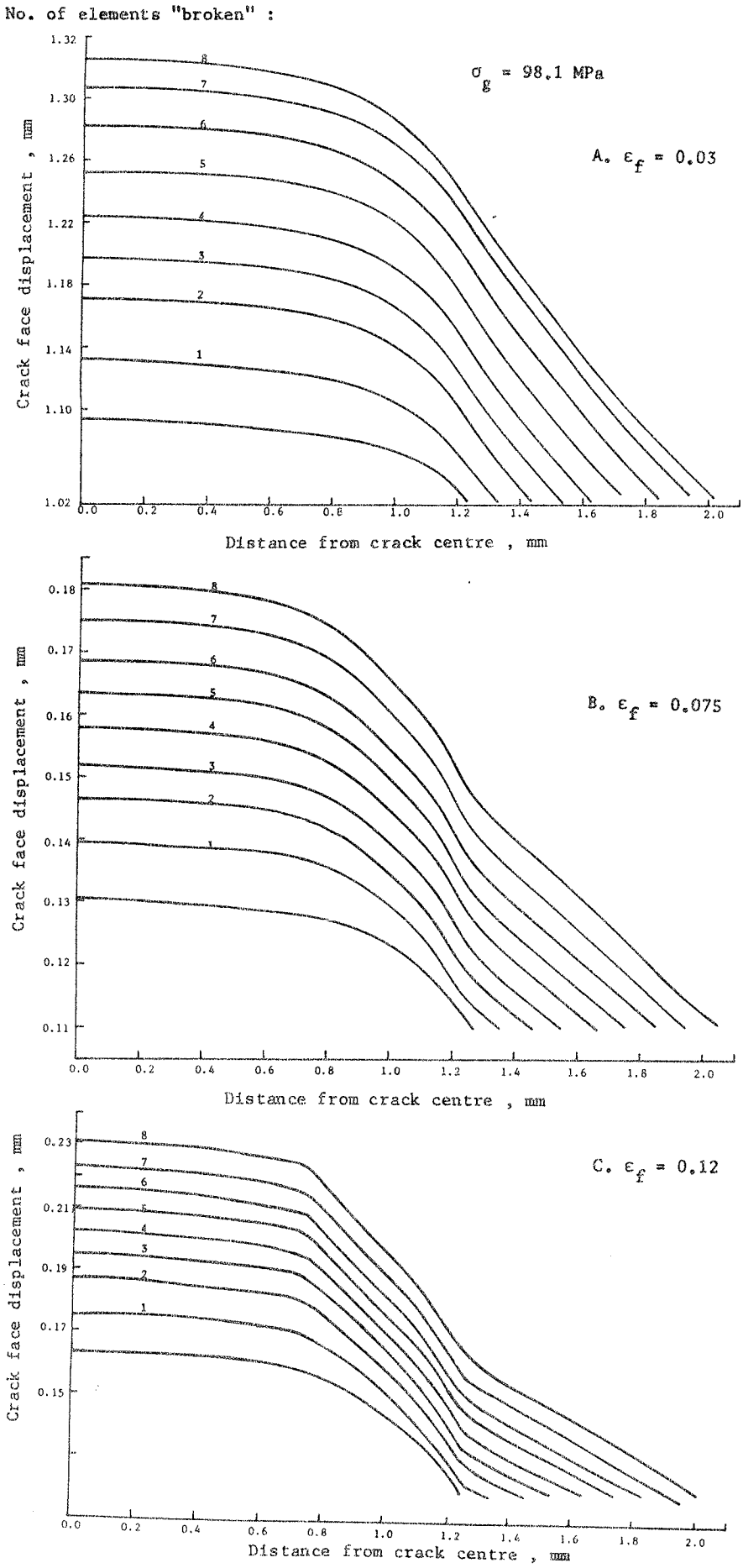

Fig. 22 Crack profiles

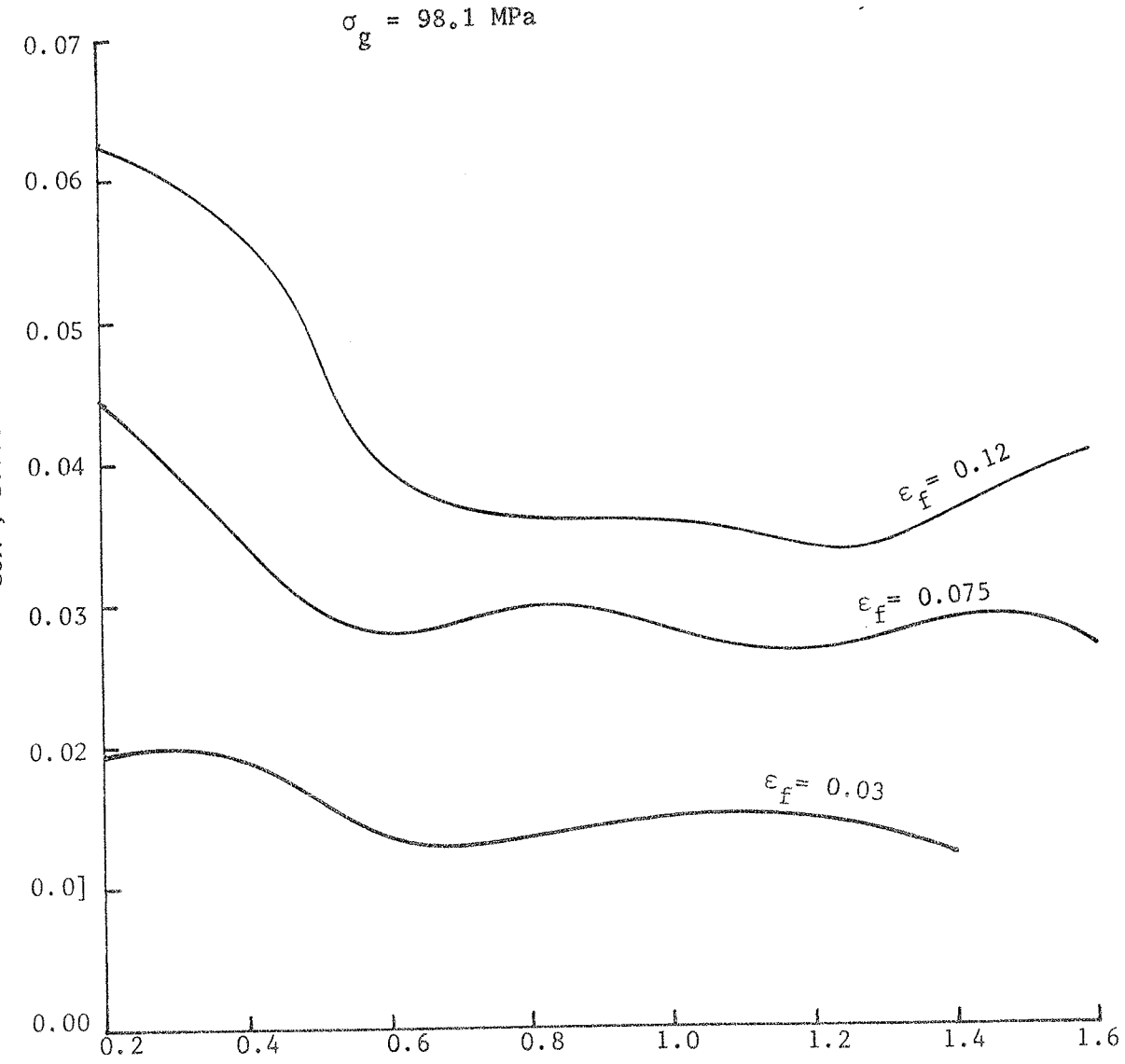

Fig. 23 Crack opening angles (COA)

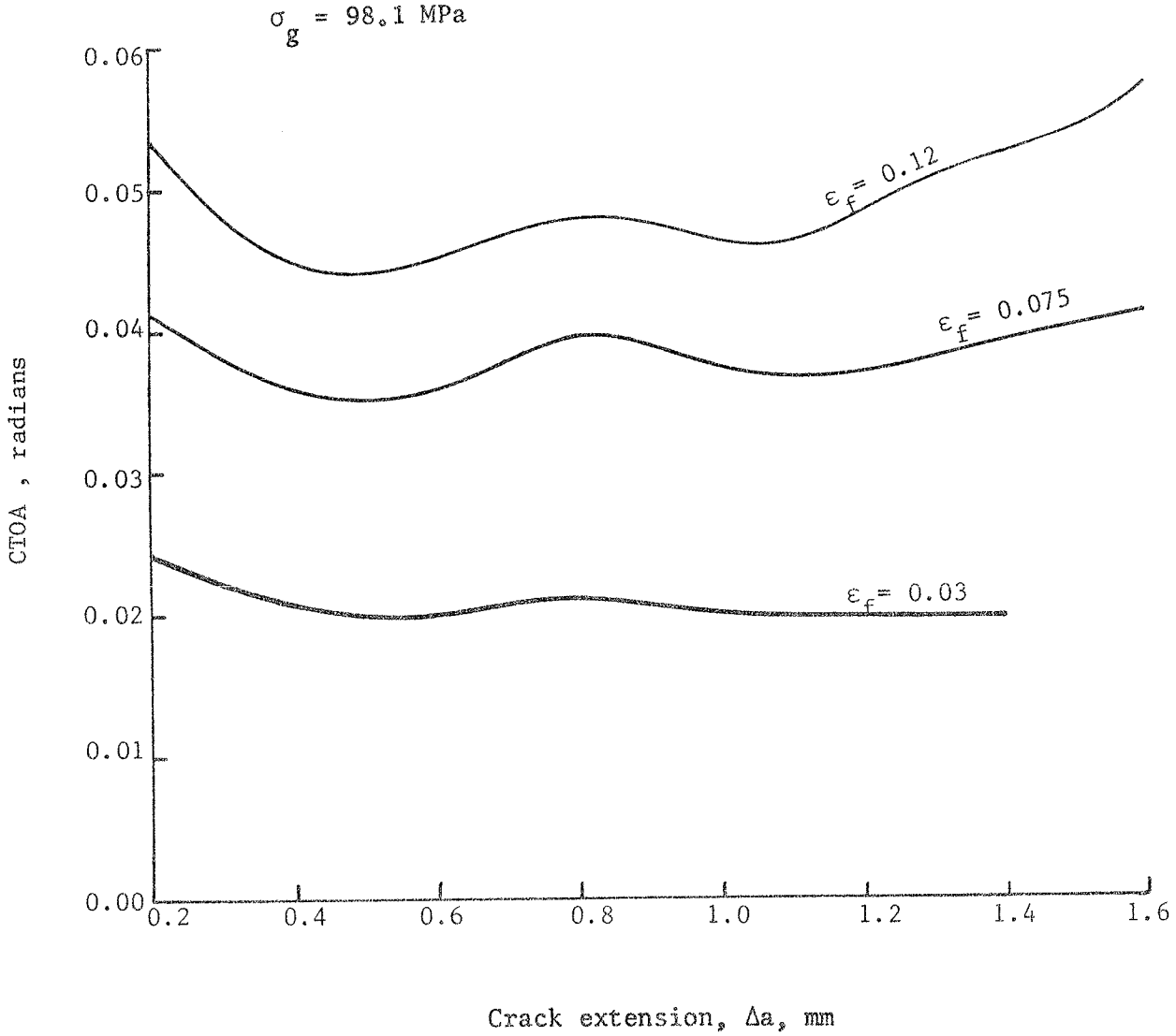

Fig. 24 Crack tip opening angles (CTOA)

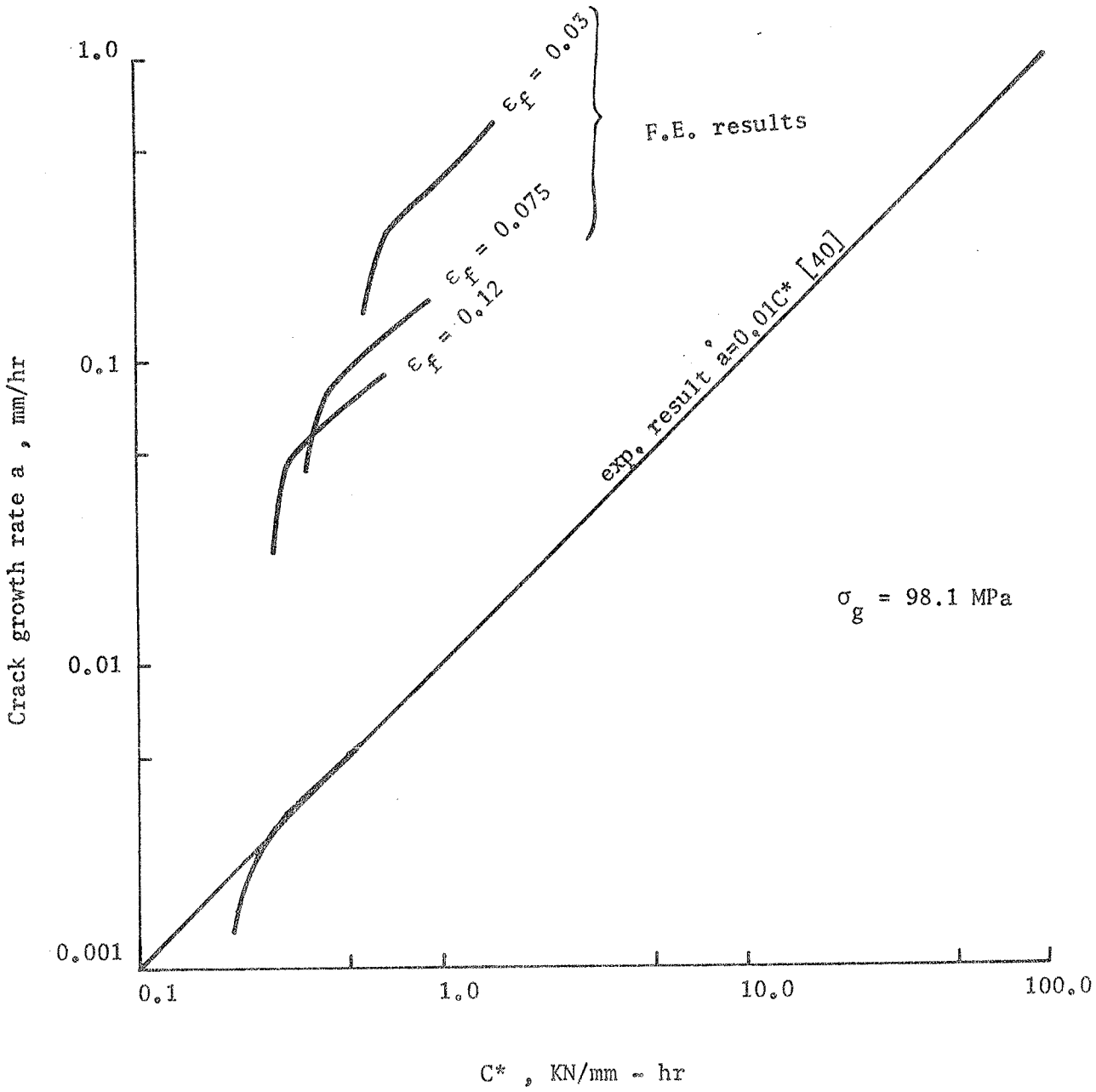

Fig. 25 Relationship between crack growth rate and the C* parameter

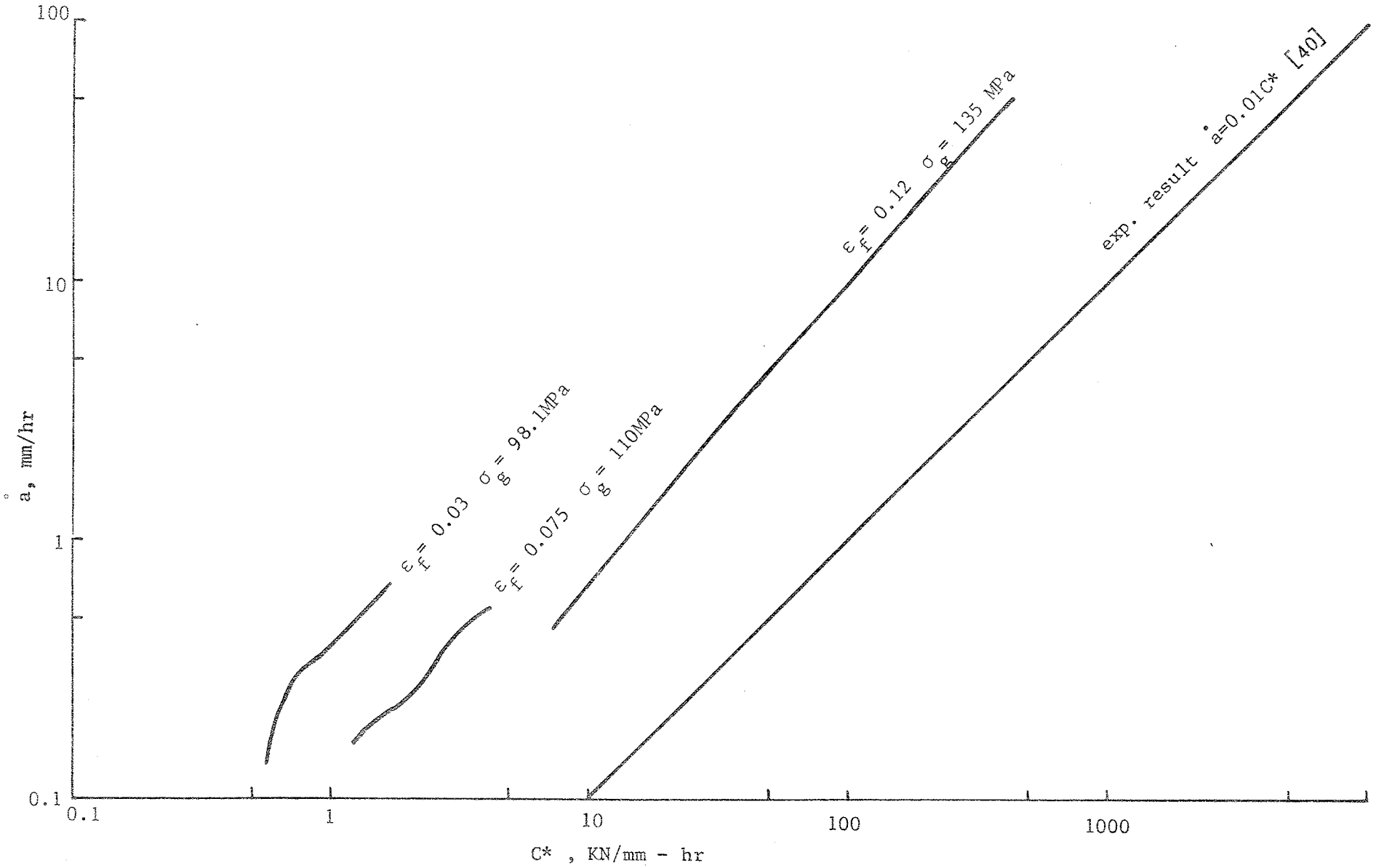

Fig.26 Relationship between crack growth rate and C* parameter as function of applied stress

TABLE 1

Mechanical Properties of 304 Stainless Steel at 650°c

Modulus of Elasticity (E)	140000 MPa*
Plastic Tangent Modulus (E')	700 MPa
Yield Strength (σ_y)	145 MPa
Ultimate Strength	310 MPa
% Elongation	60 %

* Modulus of elasticity at room temperature is 200000 MPa.